Original Research

Title: COVID-19 lung disease shares driver AT2 cytopathic features with Idiopathic pulmonary fibrosis

Authors: Saptarshi Sinha[3]*, Vanessa Castillo[3], Celia R. Espinoza[3], Courtney Tindle[3], Ayden G. Fonseca[3], Jennifer M. Dan[4, 5], Gajanan D. Katkar[3], Soumita Das[6] Debashis Sahoo[1, 2]†* and Pradipta Ghosh[3, 7]†

Affiliations:

[1]*Department of Pediatrics, University of California San Diego, La Jolla, CA, 92093.*
[2]*Department of Computer Science and Engineering, Jacobs School of Engineering, University of California San Diego, La Jolla, CA, 92093.*
[3]*Department of Cellular and Molecular Medicine, University of California San Diego, La Jolla, CA, 92093.*
[4]*Center for Infectious Disease and Vaccine Research, La Jolla Institute for Immunology (LJI), La Jolla, CA, USA.*
[5]*Department of Medicine, Division of Infectious Diseases and Global Public Health, University of California, San Diego (UCSD), La Jolla, CA, USA.*
[6]*Department of Pathology, University of California San Diego, La Jolla, CA, 92093.*
[7]*Department of Medicine, University of California San Diego, La Jolla, CA, 92093.*

*Equal contribution
† Co-Corresponding

Corresponding authors:

Debashis Sahoo, Ph.D.; Associate Professor, Department of Pediatrics, University of California San Diego; 9500 Gilman Drive, MC 0703, Leichtag Building 132; La Jolla, CA 92093-0703. **Phone:** 858-246-1803: **Fax:** 858-246-0019: **Email:** dsahoo@ucsd.edu

Pradipta Ghosh, M.D.; Professor, Departments of Medicine and Cell and Molecular Medicine, University of California San Diego; 9500 Gilman Drive (MC 0651), George E. Palade Bldg, Rm 232; La Jolla, CA 92093. **Phone**: 858-822-7633:
Email: prghosh@ucsd.edu

ABSTRACT

Background: In the aftermath of Covid-19, some patients develop a fibrotic lung disease, i.e., *p*ost-*C*OVID-19 *l*ung *d*isease (PCLD), for which we currently lack insights into pathogenesis, disease models, or treatment options.

Method: Using an AI-guided approach, we analyzed > 1000 human lung transcriptomic datasets associated with various lung conditions using two viral pandemic signatures (ViP and sViP) and one covid lung-derived signature. Upon identifying similarities between COVID-19 and idiopathic pulmonary fibrosis (IPF), we subsequently dissected the basis for such similarity from molecular, cytopathic, and immunologic perspectives using a panel of IPF-specific gene signatures, alongside signatures of alveolar type II (AT2) cytopathies and of prognostic monocyte-driven processes that are known drivers of IPF. Transcriptome-derived findings were used to construct protein- protein interaction (PPI) network to identify the major triggers of AT2 dysfunction. Key findings were validated in hamster and human adult lung organoid (ALO) pre-clinical models of COVID-19 using immunohistochemistry and qPCR.

Findings: COVID-19 resembles IPF at a fundamental level; it recapitulates the gene expression patterns (ViP and IPF signatures), cytokine storm (IL15-centric) and the AT2 cytopathic changes, e.g., injury, DNA damage, arrest in a transient, damage-induced progenitor state, and senescence-associated secretory phenotype (SASP). These immunocytopathic features were induced in pre-clinical COVID models (ALO and hamster) and reversed with effective anti-CoV-2 therapeutics in hamsters. PPI-network analyses pinpointed ER stress as one of the shared early triggers of both diseases, and IHC studies validated the same in the lungs of deceased subjects with COVID-19 and SARS-CoV-2-challenged hamster lungs. Lungs from *tg*-mice, in which ER stress is induced specifically in the AT2 cells, faithfully recapitulate the host immune response and alveolar cytopathic changes that are induced by SARS-CoV-2.

Interpretation: Like IPF, COVID-19 may be driven by injury-induced ER stress that culminates into progenitor state arrest and SASP in AT2 cells. The ViP signatures in monocytes may be key determinants of prognosis. The insights, signatures, disease models identified here are likely to spur the development of therapies for patients with IPF and other fibrotic interstitial lung disease.

Funding: This work was supported by the National Institutes for Health grants R01- GM138385 and AI155696 and funding from the Tobacco-Related disease Research Program (R01RG3780).

One Sentence Summary: Severe COVID-19 triggers cellular processes seen in fibrosing Interstitial Lung Disease

Key Words:

- Artificial Intelligence/Machine Learning
- Boolean Equivalent Clusters
- Coronavirus COVID-19
- COVID-19 lung
- Immune response
- Alveolar Type II Pneumocytes
- Damage-associated transient progenitor (DATP)
- Senescence
- ER-stress
- Interleukin 15 (IL15)

PANEL: RESEARCH IN CONTEXT

Evidence before this study

In its aftermath, the COVID-19 pandemic has left many survivors, almost a third of those who recovered, with a mysterious long-haul form of the disease which culminates in a fibrotic form of interstitial lung disease (post-COVID-19 ILD). Post-COVID-19 ILD remains a largely unknown entity. Currently we lack insights into the core cytopathic features that drives this condition.

Added value of this study

Using an AI-guided approach, which involves the use of a sets of gene signatures, protein-protein network analysis, and a hamster model of COVID-19, we have revealed here that COVID-19 -lung fibrosis resembles IPF, the most common form of ILD, at a fundamental level—showing similar gene expression patterns in the lungs and blood, and dysfunctional AT2 processes (ER stress, telomere instability, progenitor cell arrest and senescence). These findings are insightful because AT2 cells are known to contain an elegant quality control network to respond to intrinsic or extrinsic stress; a failure of such quality control results in diverse cellular phenotypes, of which ER stress appears to be a point of convergence, which appears to be sufficient to drive downstream fibrotic remodeling in the lung.

Implications of all the available evidence

Because unbiased computational methods identified the shared fundamental aspects of gene expression and cellular processes between COVID-19 and IPF, the impact of our findings is likely to go beyond COVID-19 or any viral pandemic. The insights, tools (disease models, gene signatures, and biomarkers), and mechanisms identified here are likely to spur the development of therapies for patients with IPF and other fibrotic interstitial lung disease, all of whom have limited or no treatment options. to dissect the validate prognostic biomarkers to assess and track the risk of pulmonary fibrosis and develop therapeutics to halt fibrogenic progression.

INTRODUCTION

As the acute phase of the COVID-19 pandemic winds down, the chronic diseases in its aftermath have begun to emerge. For example, many survivors are suffering from a mysterious long-haul form of the disease which culminates in a fibrotic form of interstitial lung disease (post-COVID-19 ILD)[1-9]. The actual prevalence of post-COVID-19 ILD (henceforth, *PCLD*) is still emerging; early analysis indicates that more than a third of the survivors develop fibrotic abnormalities. One of the important determinants for PCLD[10] is the duration of disease; ~4% of patients with a disease duration of less than 1 week, ~24% of patients with a disease duration between 1-3 weeks, and ~61% of patients with a disease duration > 3 weeks, developed fibrosis. Disability among survivors of severe COVID-19 has been primarily attributed to reduced lung capacities(11). While COVID-19–affected lungs and post-Influenza lungs share the histologic pattern of diffuse alveolar damage (DAD)(12) with perivascular T-cell infiltration, key differences have been observed(13). The lungs from patients with Covid-19 also showed(13): (i) widespread thrombosis with microangiopathy; (ii) severe endothelial injury associated with the presence of intracellular virus and disrupted cell membranes; and (iii) neovascularization predominantly through a mechanism of intussusceptive angiogenesis. These findings highlight that despite being viral pandemics, COVID-19, but not influenza impacts the lungs in ways that go beyond acute DAD, a common phenomenon in progressive ILDs(12). Although a recent study(14) implicated pathogenic subsets of respiratory $CD8^+$ T cells in contributing to persistent tissue microenvironment in PCLD, what remains largely unknown are some of the earliest cellular and molecular mechanisms that fuel the progression of fibrosis in COVID-19 lung (but not influenza).

As for how the fibrotic sequel of COVID-19 is managed at present, based on the shared pathological features of overt fibrosis in both end-stage COVID-19 and ILDs, lung transplantation remains the mainstay option for these patients(15-17). Although corticosteroids appear to improve the risk of PCLD(2), beyond that, there is no existing therapeutic option.

Here we seek to unravel the fundamental molecular mechanisms underlying PCLD, identifying key disease drivers (cellular processes, immune pathways, and the signaling cascades that support those pathways). We use artificial intelligence (AI) and machine learning derived gene signatures, the *Vi*ral *P*andemic, ViP and severe(s) ViP signatures that are induced in all respiratory viral pandemics(18). Besides the ViP signatures, we also use gene signatures induced in the lungs of patients with severe COVID-19. These approaches, in conjunction with experimental validation (in pre-clinical disease models and in human lung tissue) not only helped identify which lung pathology shares fundamental molecular features with COVID-19 lung, but also revealed key mechanistic insights into the pathogenesis of PCLD. The findings also provide clues into how to navigate, prognosticate and recapitulate in pre-clinical models this emergent mysterious condition. The objectivity and precision of the AI-guided unbiased approaches enhance the translational potential of our findings.

141 ## RESULTS

142 **A study design that uses gene signatures as a computational framework to navigate COVID-19 lung disease**
143 Because PCLD is still an emergent illness that lacks insights into disease pathophysiology, we resorted to a study
144 design (**Figure 1**) that is geared to achieve three goals: (i) maximize rigor by using diverse transcriptomic datasets
145 cohorts (a total of 2078 unique samples, human: 2019; mouse: 41, hamster: 18; see **Supplemental Information**
146 **1**), but (ii) minimize bias by using well characterized sets of gene signatures from independent publications (see
147 **Supplemental Information 2**), and (iii) retain objectivity and precision by using artificial intelligence/machine
148 learning (AI/ML) tools that are supported by precise mathematical algorithms and statistical tools (see *Methods*).
149 First, to ensure that the findings maintain relevance to respiratory viral pandemics and COVID-19, we
150 used a recently discovered 166-gene signature that was found to be conserved in all viral pandemics (ViP),
151 including COVID-19, and a subset of 20-genes within that signature that classifies disease severity(18); the latter
152 was found to be consistently and significantly induced in the most severe cases of COVID-19 and prognostic of
153 poor outcome, e.g., death or invasive respiratory support (see **Supplemental Information 2**). These ViP
154 signatures were rigorously validated on ~45000 datasets representing the pandemics of the past (Training datasets:
155 Influenza and avian flu; GSE47963, n = 438; GSE113211, n = 118; Validated in numerous datasets as cited
156 before) and used without further training to prospectively analyze the samples from the current pandemic (i.e.,
157 COVID-19) (**Figure 1**, *Step 0*). The ViP signatures appeared to capture the 'invariant' host response, i.e., the
158 shared fundamental nature of the host immune response induced by all viral pandemics, including COVID-19.
159 Since they were discovered, these signatures have helped navigate the emergent syndrome of multisystem
160 inflammatory syndrome in children(19) (MIS-C; a.k.a. PIMS-TS)(20).
161 We began first by using the ViP signatures as a starting computational framework to navigate the
162 syndrome of COVID-19 lung disease, in conjunction with another independently reported(13) COVID-19-lung
163 derived signature to identify idiopathic pulmonary fibrosis (IPF)(21) as a computational match for COVID-19
164 lung disease (**Figure 1**, *Step 1*). The subsequent steps in the study use the ViP signatures alongside IPF-specific
165 PBMC-derived prognostic signatures (**Figure 1**, *Step 2*) and signatures of alveolar cytopathic changes (**Figure 1**,
166 *Step 3*) to systematically assess the degree of similarities between COVID-19 lung and IPF and the crossover of
167 pathophysiologic processes in the two conditions. In the final step (**Figure 1**, *Step 4*), a set of gene signature-
168 inspired protein-protein interaction (PPI) network analysis is used which pinpointed alveolar ER stress as a
169 potential early step in both IPF and PCLD, which is sufficient to recapitulate not just the ViP signatures, but also
170 the alveolar cytopathic features that are shared between the diseases. Key predictions are validated in human lung
171 tissues and plasma from COVID-19 subjects, hamster models of COVID-19 and in human pre-clinical lung
172 models (**Figure 1**, *Steps 3-4*).

173 **COVID-19 lung disease and IPF induce a common set of gene expression signatures**

174 We first asked which pathologic lung condition comes closest to COVID-19 lung disease regarding the host
175 immune response. To this end, we used the ViP/sViP signatures (found to be induced in all CoV samples tested
176 so far(18)) and a second set of CoV-lung disease gene signatures which were derived from a differential
177 expression analysis on lung samples from healthy controls vs. fatal COVID-19(13) (see **Supplemental**
178 **Information 2**). As for the lung diseases, we ensured that all four major pathologic conditions were represented:
179 neoplastic (e.g., carcinoids and adenocarcinoma), granulomatous (e.g., tuberculosis/TB and sarcoidosis),
180 allergic/infectious (e.g., severe asthma and community acquired pneumonia/CAP and tuberculosis) and
181 vasculopathic (e.g., pulmonary hypertension/PHT and chronic thromboembolic pulmonary
182 hypertension/CTEPH) (**Figure 2A**). As expected, ViP/sViP signatures were induced in infectious diseases (CAP
183 and tuberculosis), and to our surprise, these signatures were upregulated also in sarcoidosis, a granulomatous
184 condition that progresses to fibrosis in ~20% of the patients(22, 23) (**Figure 2A**). Only two diseases (tuberculosis
185 and IPF) showed significant induction of both ViP and CoV-lung signatures, of which only one condition (IPF)
186 manifests as a diffuse disease with patchy parenchymal involvement resembling COVID-19 lung disease (**Figure**
187 **2A**).

188 We next analyzed a set of six signatures, each independently derived from diverse IPF-centric studies(24-
189 27), on diverse CoV samples; we also analyzed the ViP/sViP(18) and CoV-lung(13) signatures on 4 independent
190 single cell (scRNA seq) IPF explants. CoV samples induced the IPF signatures and IPF samples induced
191 ViP/CoV-lung signatures (**Figure 2B**). It is noteworthy that such induction of ViP/sViP signatures was
192 undetectable in the bulk RNA seq studies on IPF explants (**Supplementary Figure 1**); this is in keeping with
193 numerous reports that scRNA-seq obtains cell-level resolution in IPF that bulk-RNA seq misses(28-30). In a
194 pooled dataset (GSE149878)(31) that included both CoV and IPF samples the ViP (**Figure 2C**), sViP (**Figure**
195 **2D**), IPF-lung (**Figure 2E**) and CoV-lung (**Figure 2F**) were indistinguishably induced in both samples compared
196 to healthy controls. These results indicate that CoV and IPF signatures have crossover utility for sample
197 classification and indicate that IPF is the closest computational match to COVID-19 lung disease (**Figure 2G**).
198 Consistent with the fact that PCLD occurs in survivors of severe disease that required hospitalization(32), we
199 found that sViP signature was induced significantly higher in hospitalized compared to non-hospitalized subjects
200 (**Figure 2H**). Finally, we asked what, if any relationship exists between another poorly understood feature of
201 long-haul COVID-19, i.e., severe fatigue(33, 34). To improve rigor, we analyzed a set of other well-defined
202 fatigue syndromes (e.g., gulf war illness, chronic fatigue syndrome, and idiopathic chronic fatigue) and for
203 consistency, restricted the analysis to only whole blood/PBMC samples (**Figure 2I**). ViP/sViP and CoV-lung
204 immune signatures were induced only in CoV samples, but not in the remaining fatigue-associated syndromes
205 (**Figure 2I**), indicating that gene expression signatures in long-haul COVID-19 are distinct from other fatigue-

associated syndromes. Instead, fatigue in long-haul COVID-19 may be of similar reasons/pathophysiology that has been observed in IPF (35). It is noteworthy that profound fatigue is a shared phenomenon in both IPF and sarcoidosis(35, 36), both carry the risk of progressive fibrosis, and both conditions induce the ViP/sViP response (**Figure 2A**). These results show that COVID-19 lung is closest to IPF: both are characterized by lung fibrosis, and share gene expression patterns, suggestive of shared molecular and cellular mechanisms of disease pathogenesis.

PBMC-derived prognostic signatures in COVID-19 and IPF show crossover utility in both diseases.

Previously we showed using sc-RNA seq as well as bulk-RNA seq on sorted cells, that ViP/sViP signatures are primarily induced in COVID-19 by lung epithelial cells and myeloid cells (both alveolar macrophages and PBMCs)(18). When assessed in whole blood and/or PBMCs, the sViP signature was prognostic in COVID-19—high expression of this 20-gene signature was associated with prolonged hospital stay and mechanical ventilation(18). We noted that a PBMC-based 52-gene signature has previously been validated in numerous IPF datasets(37). In the setting of IPF, the role of PBMC-derived lung macrophages in the activation of alveolar fibroblasts has been cemented by several studies (38-43)(**Figure 3A**); the activated macrophages and myofibroblasts are thought to cross-stimulate each other, resulting in a vicious cycle that assures propagation of fibrosis throughout the lung in end-stage IPF(38, 44). Emerging studies on CoV lung have also reported the presence of pro-fibrogenic alveolar macrophages in severe COVID-19(15, 45, 46), inspiring us to investigate if the PBMC-derived prognostic signatures for IPF also prognosticate outcome in CoV, and *vice versa*.

We found that alveolar macrophages (marked by CD-14(47)) in the lungs of deceased subjects contained the viral nucleocapsid protein (**Figure 3B-C**); this is consistent with observations reported by other(48, 49). The 20-gene sViP signature was prognostic in the blood datasets from both COVID-19 (**Figure 3D**; *left*) and IPF subjects (**Figure 3D**; *middle, right*); among IPF subjects, the signature was prognostic exclusively in male subjects (**Figure 3D**; *middle*). The 52-gene 'IPF-specific' prognostic signature(37) retained its ability to prognosticate outcome in both male and female patients with IPF (as expected; **Figure 3E**; *middle, right*), but also did so in the setting of COVID-19 (**Figure 3E**; *left*). By contrast, the CoV-lung tissue-derived signature that is known to distinguish CoV from both healthy and influenza-affected lungs(50), did not prognosticate outcome in either COVID-19 (**Figure 3F**; *left*) or IPF subjects (**Figure 3F**; *middle vs. right*). It indicates that the PBMC-derived signatures in CoV and IPF retain their prognostic relevance in both conditions, with at least one key notable difference; sViP, but not the IPF signature revealed the well-established gender specific differences in the progression of IPF. These results indicate that PBMCs in both IPF and COVID-19 have similar gene induction patterns, and that the cross-over prognostic value of IPF- and sViP signatures induced in the PBMCs may reflect the profibrogenic immune response that is shared in both conditions.

239 **Alveolar type II (AT2) telomere dysfunction and senescence are shared features in both COVID-19 and**
240 **IPF**.

241 Besides the contributions from PBMCs, a contemporary paradigm in IPF is that chronic injury to distal lung tissue
242 leads to either loss or altered function of epithelial stem cells (i.e., AT2 cells), that promote dysregulated repair
243 and pathogenic activation of fibroblasts.(51-53) We asked if the AT2 dysfunction states previously reported in
244 IPF also occur in COVID-19. To this end, we analyzed a single cell dataset of bronchoalveolar lavage from
245 COVID-19 patients (GSE145926) for the induction of ViP/sViP, CoV-lung and IPF signatures and other
246 signatures that are indicative of three important AT2 cytopathies: (i) Damage associated transient progenitor
247 (DATP(54)), a distinct *KRT8*+/*CLDN4*+ AT2 lineage that has been independently shown, nearly simultaneously
248 by 3 independent groups(54-56) to be associated with activated myofibroblasts during lung fibrosis in the setting
249 of IPF(53). (ii) AT2-senescence signature, which was derived from another IPF-focused study(57) that used
250 human and mouse models to pinpoint Doxycycline-induced program of p53-dependent cellular senescence, AT2
251 cell depletion, and spontaneous, progressive pulmonary fibrosis; and (iii) Aging associated telomerase
252 dysfunction (TERC_UP) signature, which was derived from aging telomerase knockout (*Terc*$^{-/-}$) mice. We found
253 that the entire panel of signatures analyzed were upregulated, most consistently, only in the epithelial cells (**Figure**
254 **4A**), whereas only some were induced and not others in the non-epithelial compartments.

255 We next confirmed that a composite score of *IL15/IL15RA*, AT2-senescence and telomerase dysfunction
256 (TERC_UP) signatures were induced indistinguishably in both CoV and IPF samples compared to healthy
257 controls (**Figure 4B**). A correlation matrix (**Figure 4C**) on the entire cohort showed that while both IL15 and
258 IL15RA correlate with the ViP signature (as expected), IL15RA, but not IL15 correlate with TERC_UP and AT2-
259 senescence signatures. Both ViP and sViP signatures correlate with AT2 senescence. Furthermore, when we
260 tested AT2-senescence and telomere dysfunction in other CoV datasets, we found that these features were
261 conserved in most CoV samples across diverse cohorts (**Figure 4D**). An independent sc-RNA seq IPF dataset
262 further confirmed that, much like CoV lung, the induction of ViP/sViP in alveolar epithelium (EpCAM+; **Figure**
263 **4E**) is associated with IL15/IL15RA induction, AT2-senescence and telomere dysfunction. These findings
264 support the existence of telomere dysfunction and DNA damage in both acute COVID-19 and IPF.

265

266 **Hamsters, but not mice recapitulate the host immune response and AT2 cytopathic features of COVID-19**

267 Evidence suggests that there is a wide gap between COVID-19 in humans and animal models(58); interspecies-
268 related differences, such as host specificity and divergent immune responses can lead to misinterpretation. To
269 objectively assess which model improves the translational potential of any discovery from this study, we curated
270 all publicly available transcriptomic datasets from pre-clinical rodent models of COVID-19 and analyzed them for

271 the induction of the ViP/sViP, IL15/IL15RA composite score, CoV-lung, IPF signatures and signatures of AT2
272 senescence and transition-state arrest (DATP) (**Supplementary Figure S2A**). We saw that the golden Syrian
273 hamsters, but not the humanized transgenic mouse models (**Supplementary Figure S2A**; *bottom*) induce most, if
274 not all the key signatures upon SARS-CoV-2 challenge (**Supplementary Figure S2A**; *top*). Most importantly, all
275 signatures (**Supplementary Figure S2A**; *top*), including that of AT2-damage associated transient progenitor
276 population (**Supplementary Figure S2B**; DATP) were effectively reversed with two therapeutic approaches. The
277 first approach was the use of N-hydroxycytidine, the parent of the prodrug MK-4482 (Molnupiravir, EIDD-2801)
278 which has not only proven as a potent and selective oral antiviral nucleoside analogue in mice, guinea pigs, ferrets
279 and human airway epithelium organoids(59-64), but also showed promise in Phase IIa trials in the treatment of
280 COVID-19 patients (NCT04405570(65)). both biologic and directly acting anti-viral therapies. The second
281 approach was the use of SARS-CoV-2-neutralizing antibodies whose design was inspired by monoclonal
282 antibodies (mAbs) isolated from from convalescent donors(66). A specific isotype of this antibody, which binds
283 to the receptor-binding domain (RBD-A) of SARS-CoV-2 spike protein in a fashion that precludes binding to
284 host ACE2, was demonstrated as effective in preventing infection and weight loss symptoms, in cell-based and
285 *in vivo* hamster models of infection, respectively.

286 These findings show that hamster lungs best recapitulate the host immune response, the nature of the
287 cytokine storm (IL15-centric), and the AT2 cytopathies that are shared between COVID-19 and IPF. It is also in
288 keeping with emerging data that Syrian hamsters best emulate COVID-19(58); they also recapitulate progressive
289 fibrosis in IPF(67).

290

291 **Validation of the predicted AT2 cytopathic features of COVID-19 in hamster and human lungs**

292 We next sought to determine if the SARS-CoV-2 virus can induce the AT2 cytopathic changes, and whether
293 effective therapeutics can abrogate those changes. We analyzed by RNA seq and trichrome stain the lungs from
294 SARS-CoV-2-challenged golden Syrian hamsters who were pre-treated either with EIDD-2801 or anti-Spike
295 (CoV-2) mAb or untreated controls (see study protocol in **Figure 5A**). Key genes associated with AT2 senescence
296 (*Tp53* and *Cdkn2a*), ER stress (*Hspa5/Grp78*), DATP (*Krt8* and *Cldn4*) and fibrosis (*Col1a, Col3a* and *Serpine1*)
297 were all induced in the infected lungs (compared to uninfected controls) but not in those that were treated (**Figure
298 5B**). Trichrome staining confirmed that compared to uninfected controls, collagen deposition was induced in the
299 infected lungs, but not in those that were treated (**Figure 5C-D**). Immunohistology studies confirmed that Cdkn2a,
300 Krt8, Cldn4 and Tp53 proteins were expressed in the injured alveoli, but not in the treated lungs (**Figure 5E-F**).

301 We next confirmed extensive deposition of eosin-positive collagenous materials in lung tissues obtained
302 at rapid autopsies on deceased subjects with COVID-19 compared to normal lung tissues (**Figure 6A**; *top*). KRT8
303 and TP53 were also induced in the COVID-19 lungs (**Figure 6A**; *middle* and *bottom*). Finally, plasma ELISA

304 studies in a cohort of symptomatic COVID-19 patients who presented to the UC San Diego Medical Center with
305 varying disease severity, ranging from mild to fatal (see **Supplemental Information 3-4**), we detected several
306 cellular senescence-associated cytokines during the acute compared to the convalescent visit (**Figure 6B;**
307 **Supplementary Figure S3**). It is noteworthy that VEGF, TNFα, IL6 and IL1β, all cytokines that have been
308 implicated in the fibrotic process post-COVID-19 (reviewed in(68)) were significantly elevated only in the most
309 critical form of the disease. Findings are also consistent with the fact that VEGF-targeted therapeutics
310 (Bevacizumab) in COVD-19 patients improved lung oxygenation up to day 28 during follow-up(69).

311 We next asked if the key aspects of the host immune response and AT2 cytopathic changes are induced
312 in the various human pre-clinical *in vitro* models of COVID-19. We assessed our published models of COVID-
313 19-in-a-dish(70) (**Figure 6C, 6D-***top 4 rows*) for AT2-senescence and for their ability to mimic the unique milieu
314 in COVID-19 lungs(13). We also analyzed CoV2-challenged primary(p)AT2 and A549 cells (**Figure 6D-***bottom*
315 *3 rows*). We found that submerged monolayers of adult lung organoids (ALO mono), which were previously
316 found to outperform fetal lung organoids(71) and other models in recapitulating the gene expression signatures
317 observed in human COVID-19 lungs(70), also outperformed here. While most models induced some signatures,
318 the submerged ALO model induced them all (**Figure 6D**).
319

320 **Protein-protein network analysis predicts AT2 ER stress as an early initiating event in COVID-19**

321 To identify some of the earliest AT2 cell processes that might be triggered as a consequence of the host immune
322 response in acute COVID-19, which may precede the development of transient state arrest and senescence, we
323 resorted to a PPI network analysis. To this end, we used the genes in the sViP(18), AT2 senescence(57) and
324 DATP(54) and DATP(54) signatures as 'seed' nodes to fetch additional connecting nodes from human protein-
325 protein interactions in STRING database(72) (**Figure 7A;** see **Supplemental Information 5)**. Once built, we
326 assessed the network for degrees of connectivity (**Figure 7B**; *left*) and representation of cellular processes in the
327 most connected nodes by using two approaches: CluGo analysis(73) (**Figure 7B**; *right*) and Reactome pathway
328 analysis(74) (**Figure 7C**). While CluGO analysis showed an overrepresentation of proteins associated unfolded
329 protein response, ER stress, regulation of telomerase, regulation of cell aging and regulation of G1/S phase
330 transition (**Figure 7B**; *right*), reactome analysis showed enrichment of pathways associated with senescence
331 (**Figure 7C**; *red*), platelet activation and degranulation (**Figure 7C**; *blue*), and Tp53-dependent DNA damage
332 response (**Figure 7B**; *green*). That platelet activation (indicative of a prothrombotic state) is captured within the
333 PPI network is in keeping with what appears to be a hallmark of PCLD(13). Numerous independent observations
334 in diverse cohorts of patients have now confirmed that platelet dysfunction amplifies endotheliopathy in COVID-
335 19(75) and that a vicious cycle of thromboinflammation, endothelial dysfunction and immunothrombosis are key
336 pathogenic mechanisms in COVID-19(76, 77). It is noteworthy, that we found that levels of IL6 and platelets

showed significant negative correlation (**Supplementary Figure 3**). Because IL6 has been specifically implicated in platelet hyper-reactivity and thrombosis(78), as well as in thrombus resolution(79), the strong negative correlation may suggest the presence of thromboinflammation; the latter is one of the first and most distinctive pathological feature of CoV-lung to be reported since the beginning of this pandemic(13). As for AT2-centric processes, the PPI network analyses suggest that ER stress, which has been shown to serve as a causal role for profibrogenic epithelial states (SASP) that is shared between aging-associated pulmonary fibrosis and IPF(80), may also be a common underlying factor in fibrotic COVID-19 lung disease.

ER stress in AT2 cells is observed in COVID-19 and is sufficient to recapitulate the host immune response in COVID-19 and IPF. We next sought to investigate if alveolar ER stress is a feature in CoV-lung. To this end, we analyzed infected human (**Figure 8A**) and hamster (**Figure 8B**) lungs for the ER chaperone *Grp78*, a key regulator of ER homeostasis expression by IHC. We found that compared to normal uninfected lungs, infected lungs showed a significant increase in Grp78 staining and that the intensity of such staining was highest in the epithelial cells lining the alveolar spaces in both species (**Figure 8A-B**).

To determine if ER stress in AT2 cells may contribute to the epithelial dysfunction and fibrosis that is observed as a sequel of COVID-19, we leveraged a previously characterized *tg*-mouse model of AT2-specific conditional [tamoxifen (Tmx)-inducible] deletion of Grp78 ($Sftpc^{+/creERT2};Grp78^{f/f}$)(80). These mice are known to lose weight and die (more pronounced in male and old mice) due to lung inflammation, and spatially heterogeneous fibrosis characterized by fibroblastic foci and hyperplastic AT2 cells, all features of IPF(80). We found that compared to their littermate controls, lungs from these mice (unlike other transgenic mouse models of COVID-19; see **Figure S2A**) induced the ViP/sViP, CoV2-lung and IPF signatures, as well as the AT2 cytopathic changes such as DATP and AT2 senescence (**Figure 8C**; *bottom row*). In fact, the pattern of gene expression was similar to SARS-CoV-2-challenged hamster lungs (**Figure 8C**; *top row*). These findings indicate that ER stress is sufficient to faithfully recapitulate the host immune response and alveolar cytopathic changes that are observed in COVID-19 lung disease and IPF.

362 **DISCUSSION**

363 The major discovery we report here is that lung disease in severe COVID-19 resembles IPF, the most common
364 form of ILD, at a fundamental level—showing similar gene expression patterns (ViP and IPF signatures), shared
365 prognostic signatures (in circulating PBMCs), dysfunctional cell states (AT2 and monocytes), and dysfunctional
366 AT2 processes (ER stress, telomere instability and senescence)]. Our findings support the following model (see
367 **Figure 8D**): Upon injury (viral infection/inflammatory cytokines), diffuse alveolar damage is associated with
368 extensive loss of AT1 cells, which are duly replaced by AT2 cells serve as progenitors that are capable of self-
369 renewal and differentiation into AT1 cells(81-83). But such physiologic regeneration and healing process is
370 impaired when AT2 progenitors are also injured and begin to elicit ER stress responses, which induces telomerase
371 activity(84, 85). Because severe COVID-19 has been linked to short telomere lengths(85) [not as a cause, i.e,
372 SARS-CoV-2 infection does not shorten telomeres, but as a predisposition(86)], it is possible that patients who
373 have short and/or dysfunctional telomeres fail to adequately respond to ER stress, and instead, become senescent
374 (through p53 activation), accumulate DNA damage and enter a dysfunctional *KRT8+* transitional stem cell
375 state(87). The latter is a phenomenon that has been independently reported by three groups, under different names:
376 PATS, pre-alveolar type-1 transitional cell state(56); ADI, alveolar differentiation intermediates(55); DATP,
377 damage-associated transient progenitors(54). All three groups reported their presence in fibrotic regions of IPF
378 lungs; an increase of AT2 cells in the transitional state was invariably accompanied by an increase in
379 myofibroblasts. Our PPI network analyses suggested that AT2 senescence and progenitor arrested state in the
380 setting of a ViP/sViP-immune response (cytokine storm contributed by PBMCs) may support a SASP phenotype,
381 which is a pathological feature of aging and IPF lung(88, 89). It is possible that fibroblasts/myofibroblasts also
382 contribute to this vicious cycle of inflammation and AT2 dysfunction. These findings show that these two distinct
383 clinical syndromes, IPF, which predates the current pandemic by many decades, and the novel COVID-19, share
384 a similar profile of host immune response, both in the lung microenvironment (in AT2 cells, to be specific) as
385 well as in the circulating blood/PBMCs. We not only formally define the nature of that host response and provide
386 computational tools to measure the extent of such response, but also chart the cascade of cytopathic changes in
387 the alveoli that are critical for the profibrogenic state. It is noteworthy that the same host immune response is seen
388 also in MIS-C, a new disease that co-emerged with COVID-19, and in KD (which shares overlapping features
389 with MIS-C in clinical presentation(90)).
390

391 There are three major impacts and/implications of the findings reported in this study. First, our finding
392 that COVID-19 and IPF share fundamental host immune response and alveolar cytopathic features is in keeping
393 with the fact that both diseases share epidemiologic similarities—they primarily impact older adults, males more
394 than females, and is characterized by progressive worsening of dyspnea and lung function(91, 92). The induction

395 of ViP/sViP signatures in IPF is consistent with gathering consensus in the past decade that IPF may be a multi-
396 trigger infection-driven chronic inflammatory condition (21, 93-95). Finally, patients with existing ILDs have
397 greater odds of death due to COVID-19 compared with adults without ILD, even after controlling for age, sex,
398 and comorbidities(96-98). At day 30 of COVID-19, 35% of patients with fibrotic idiopathic ILD had died
399 compared with 19% of those with other ILDs(99). Whether the shared molecular or pathophysiologic features we
400 report here synergize to increase fatality remains unknown; however, these shared features support the
401 rationalization of clinical trials in COVID-19 using FDA-approved drugs for IPF, nintedanib (Ofev®) and
402 pirfenidone (Esbriet®) (NCT04856111 and NCT04653831), and anecdotal case reports and case series have
403 already chronicled the benefits of their use in COVID-19 lung disease(100-102).
404
405 Second, most severe COVID-19 patients develop pneumonia and hyperinflammation likely related to a
406 macrophage activation syndrome(103) commonly named "cytokine storm". Although this storm has been
407 implicated(104), and it is comprised of the generic mix of all the typical cytokines(10), which exact component
408 is the pro-fibrogenic driver remains unclear. By showing that a IL15/IL15RA-centric cytokine storm is the key
409 shared phenomenon between CoV and IPF lungs, this study provides a link between hyperinflammation and the
410 sequelae of fibrosis. Findings are consistent with prior reports of circulating IL15 as a biomarker for
411 prognostication in IPF and other ILDs(105-107). As for what may be contributing to such a cytokine response,
412 myeloid cells are likely to be major culprits, but dysfunctional AT2 cells cannot be ruled out. Prior studies using
413 bleomycin-challenged transgenic mice that lacks the *Telomeric Repeat Binding Factor 2* in the AT2 cells
414 (*Trf2*$^{Fl/Fl}$*;Sftpc-CreER*) have shown that AT2 cells with telomere dysfunction upregulate an IL15-centric
415 pathways(108). Mutations in the two main components of the telomerase holoenzyme complex that is responsible
416 forcreating new telomeric DNA, *Telomerase reverse transcriptase (TERT)* or *telomerase RNA (TERC),* are major
417 monogenic causes of pulmonary fibrosis(109). Patients with IPF have shortened telomeres; short telomeres and
418 TERT/TERC-disease associated variants were associated with specific clinical and biological features and
419 reduced transplant-free survival (109, 110). Similarly, short telomeres increase the risk of severe COVID-19(86,
420 111, 112), pulmonary fibrosis and poorer outcomes(112, 113). It is possible that injury, DNA damage and IL15
421 signalling in AT2 cells are one component in the profibrogenic cascade and suggest that IL15-targeted
422 therapeutics may be beneficial in the most severe cases of COVID-19 to prevent fibrotic sequelae.
423
424 Third, our finding that shared alveolar cytopathic changes (e.g., DNA damage, progenitor state arrest,
425 SASP, and ER stress) fuel fibrogenic programs in both COVID-19 and IPF are insightful because AT2 cells are
426 known to contain an elegant quality control feedback loop to respond to intrinsic or extrinsic stress; a failure of
427 such quality control results in diverse cellular phenotypes (reviewed in (114)): ER stress (115), defective

428 autophagy, mitochondrial dysfunction, apoptosis, inflammatory cell recruitment, profibrotic signaling, and
429 altered progenitor function(87, 116, 117) that ultimately converge to drive downstream fibrotic remodeling in the
430 lung. Prior work(57), which led to the discovery of the AT2-senescence signature (which we used here), had
431 demonstrated that senescence of AT2 cells (not loss of AT2) is sufficient to drive progressive pulmonary fibrosis.
432 Others agree, and this is now an established pathophysiologic trigger in lung fibrosis(51, 118-120). Our findings
433 are in keeping with published work(121) that suggest that AT2 senescence may be a targetable disease driver of
434 lung injury in COVID-19. Although AT2 senescence is a shared phenomenon, our PPI network analyses --which
435 integrated AT2 processes with the immune responses (ViP signatures) -- provided valuable clues into how platelet
436 activation and thromboinflammation may be uniquely seen in the setting of COVID-19. These findings are in
437 keeping with recent publications(122-124) which suggest that SARS-CoV-2 could induce epithelial senescence;
438 senescencet AT2 cells would then assume a SASP phenotype, which in turn led to neutrophil and platelet
439 activation, and activation of the clotting cascade(122).
440
441 As for the limitations of this study, it remains unclear how to model progressive lung fibrosis *in vitro* and
442 hence, no attempt was made to do so. Our results suggest that AT2 cells alone may be insufficient for such
443 modeling because a specific host immune response that is carried in the PBMCs is a clear determinant as to who
444 progresses and who does not. Although AT2-specific modulation of ER-stress pathway and SARS-CoV-
445 challenged (treated vs untreated) hamsters were used to go beyond association and establish causation, our study
446 did not attempt to inhibit/reverse fibrosis in COVID-19 by acting on any profibrogenic cellular pathway/process.
447 Development of novel chemical matter/biologicals and validation of the therapeutic efficacy of such agents will
448 take time, but if successful, our findings show that their benefits will likely transcend beyond PCLD into IPF and
449 other fibrotic lung conditions such as IPF.
450
451 In conclusion, this transdisciplinary work provides insights into the pathogenesis of PCLD, formally
452 defines the fibrogenic processes in the lung, and rigorously validates high value gene signatures or even targets
453 (i.e., IL15, senescence pathways, etc.) to track and manipulate the same. The insights, tools, computationally
454 vetted disease models and biomarkers (prognostic gene signatures) identified here are likely to spur the
455 development of therapies for patients with fibrotic interstitial lung disease of diverse causes, including IPF, all of
456 whom have limited or no good treatment options.

457 # METHODS

458 ## KEY RESOURCE TABLE:

MATERIALS & REAGENTS			
ANTIBODIES USED FOR IMMUNOCYTOCHEMISTRY			
Name	**Manufacturer**	**Catalog number**	**Dilution factor**
p14 ARF (E3X6D)	Cell Signaling	74560S	1:250
GRP78/BIP Rabbit polyclonal antibody	Proteintech	11587-1-AP	1:500
P53 Rabbit polyclonal antibody	Proteintech	21891-1-AP	1:200
Cytokeratin 8 Rabbit polyclonal antibody	Proteintech	10384-1-AP	1:2000
Claudin 4-specific Rabbit polyclonal antibody	Proteintech	16195-1-AP	1:200
p21 Waf1 / Cip1 (12D1)	Cell Signaling	2947S	1:50
INSTRUMENTS			
Leica DMI4000B (Automated Inverted Microscope)	Leica Microsystems	DMI4000B	
Power Pressure Cooker XL	Tristar Products		
MESO QuickPlex SQ 120	PBL Assay Science		
SOFTWARE & PACKAGES			
ImageJ	https://imagej.nih.gov/ij/index.html		
GraphPad Prism	https://www.graphpad.com/scientific-software/prism/		
MSD® DISCOVERY WORKBENCH 4.0	https://www.mesoscale.com/en/products_and_services/software/		
NetworkX	https://networkx.org		
Cytoscape	https://cytoscape.org		
KITS, ENZYMES, CHEMICALS, AND REAGENTS			
Zinc Formalin	Fisher Scientific	23-313096	
Xylene	VWR	XX0060-4	
Hematoxylin	BioGenex	HK100-9K	
Two-Component DAB	BioGenex	HK542-XAKE	2 drops per 1mL
Ethanol	Koptec	UN1170	
Sodium Citrate	Sigma-Aldrich	W302600	
Tris Base	Fisher Scientific	BP154-1	
Ethylenediaminetetraacetic acid (EDTA)	Fischer Scientific	BP118-500	
3% Hydrogen Peroxide	Target	245-07-3628	
ImmPRESS HRP Horse Anti-Rabbit IgG Polymer Detection Kit, Peroxidase	Vector Labs	MP-7401	
Goat serum 2.5%	Vector Laboratories	S-10120	
Normal Antibody Diluent	MP Biomedicals, LLC	980641	

459 **DETAILED METHODS:**

460 ***Computational Methods***

461

462 **ViP and severe (s)ViP Signatures**

463 ViP (Viral Pandemic) signature(18) is derived from a list of 166 genes using Boolean Analysis of large viral
464 infection datasets (training datasets: GSE47963, n = 438; GSE113211, n = 118). This 166-gene signature was
465 conserved in all viral pandemics, including COVID-19, inspiring the nomenclatures ViP signature. A subset of
466 20-genes classified disease severity called severe-ViP signature using an additional cohort (GSE101702, n =
467 159)(18). No interstitial lung disease (ILD) datasets, or for that matter any other lung dataset was used during the
468 process of discovery and validation of the ViP/sViP signatures. To compute the ViP signature, first the genes
469 present in this list were normalized according to a modified Z-score approach centered around StepMiner
470 threshold (formula = (expr -SThr)/3*stddev). The normalized expression values for every probeset for 166 genes
471 were added together to create the final ViP signature. The severe ViP signature is computed similarly using 20
472 genes. The samples were ordered finally based on both the ViP and severe-ViP signature. A color-coded bar plot
473 is combined with a violin plot to visualize the gene signature-based classification.

474

475 **Protein-protein interaction network (PPIN) construction**

476 PPIN has been constructed using the gene signatures as a set of seed nodes. The nodes between the seed nodes
477 were fetched using the connecting shortest paths and their components from the human protein interaction dataset
478 of the STRING database(72). A high cutoff of STRING interaction score has been chosen based on the proteins
479 present in the signature list to neglect the false positive interactions.

480

481 **Data analysis**

482 Several publicly available microarrays and RNASeq databases were downloaded from the National Center for
483 Biotechnology Information (NCBI) Gene Expression Omnibus (GEO) website.(125-127) Gene expression
484 summarization was performed by normalizing Affymetrix platforms by RMA (Robust Multichip Average)[81, 82]
485 and RNASeq platforms by computing TPM (Transcripts Per Millions) (49, 128) values whenever normalized data
486 were not available in GEO. We used log2(TPM +1) as the final gene expression value for analyses. GEO
487 accession numbers are reported in figures, and text. A catalog of all datasets analyzed in this work can be
488 found in **Supplementary Table 1.** StepMiner analysis and methodologies for composite gene signatures, outcome
489 analyses, and violin plots are detailed in Supplementary Online Methods.

490

491 **Statistical Analyses**

492 Gene signature is used to classify sample categories and the performance of the multi- class classification is
493 measured by ROC-AUC (Receiver Operating Characteristics Area Under the Curve) values. A color-coded bar
494 plot is combined with a density plot to visualize the gene signature-based classification.All statistical tests were
495 performed using R version 3.2.3 (2015-12-10). Standard t-tests were performed using python scipy.stats.ttest_ind
496 package (version 0.19.0) with Welch's Two Sample t-test (unpaired, unequalvariance (equal_var=False),
497 and unequal sample size) parameters. Multiple hypothesis correction was performed by adjusting *p* values with
498 statsmodels.stats.multitest.multipletests (fdr_bh: Benjamini/Hochberg principles). Pathway analysis of gene lists
499 were carried out via the Reactome database and CluGo algorithm. Reactome identifiessignaling and metabolic
500 molecules and organizes their relations into biological pathways and processes. Kaplan- Meier analysis is
501 performed using lifelines python package version 0.14.6. Violin, Swarm and Bubble plots are created using
502 python seaborn package version 0.10.1. The source code for Boolean analysis framework is available at
503 https://github.com/sahoo00/BoNE(129) and https://github.com/sahoo00/Hegemon(130).
504

505 ***Experimental Methods***

506 **Rapid autopsy procedure for tissue collection**

507 The lung specimens from the COVID-19 positive human subjects were collected as described in detail previously
508 (18, 70) using autopsy (study was IRB Exempt). All donations to this trial were obtained after telephone consent
509 followed by written email confirmation with next of kin/power of attorney per California state law (no in-person
510 visitation could be allowed into our COVID-19 ICU during the pandemic). The team member followed the CDC
511 guidelines for COVID-19 and the autopsy procedures[8, 9]. Lung specimens were collected in 10% Zinc-formalin
512 and stored for 72 h before processing for histology. Autopsy #2 was a standard autopsy performed by anatomical
513 pathology in the BSL3 autopsy suite. The patient expired and his family consented for autopsy. After 48 hours,
514 lungs were removed and immersion fixed whole in 10% formalin for 48 hours and then processed further. Lungs
515 were only partially fixed at this time (about 50% fixed in thicker segments) and were sectioned further into small
516 2-4cm chunks and immersed in 10% formalin for further investigation. Autopsies #4 and #5 were collected from
517 rapid postmortem lung biopsies. The procedure was performed in the Jacobs Medical Center ICU (all the ICU
518 rooms have a pressure-negative environment, with air exhausted through HEPA filters [Biosafety Level 3 (BSL3)]
519 for isolation of SARS-CoV-2 virus). Biopsies were performed 2-4 hours after patient expiration. Ventilator was
520 shut off to reduce aerosolization of viral particles at least 1 hour after loss of pulse and before the sample
521 collection. Every team member had personal protective equipment in accordance with the University policies for
522 procedures on patients with COVID-19 (N95 mask + surgical mask, hairnet, full face shield, surgical gowns,
523 double surgical gloves, booties). Lung biopsies were obtained after L-thoracotomy in the 5th intercostal space by

524 our cardiothoracic surgery team. Samples were taken from the left upper lobe (LUL) and left lower lobe (LLL)
525 and then sectioned further.
526
527 **Collection of blood from COVID-19 patients**
528 Blood from COVID-19 donors was either obtained at a UC San Diego Health clinic under the approved IRB
529 protocols of the University of California, San Diego (UCSD; 200236X) or recruited at the La Jolla Institute under
530 IRB approved (LJI; VD-214). COVID-19 donors were California residents, who were either referred to the study
531 by a health care provider or self-referred. Blood was collected in acid citrate dextrose (ACD) tubes (UCSD) or in
532 EDTA tubes (LJI) and stored at room temperature prior to processing for plasma collection. Seropositivity against
533 SARS-CoV-2 was confirmed by ELISA. At the time of enrollment, all COVID-19 donors provided written
534 informed consent to participate in the present and future studies. Patient characteristic is listed in Supplemental
535 Information 3.
536
537 **Human serum cytokines measurement**
538 Human serum cytokines measurement was performed using the V-PLEX Custom Human Biomarkers from MSD
539 platform [MESO QuickPlex SQ 120]. Human serum samples fractionated from peripheral blood of KD and MIS-
540 C patients (all samples collected prior to the initiation of treatments) were analyzed using customized standard
541 multiplex plates as per the manufacturer's instructions using recommended software [MSD® DISCOVERY
542 WORKBENCH 4.0].
543
544 **COVID-19 lung models in-a-dish**
545 Monolayers derived from adult lung organoids (ALOs), primary airway cells, or hiPSC-derived alveolar type II
546 (AT2) pneumocytes were infected with SARS-CoV-2 to create in vitro lung models of COVID-19 as described
547 previously(70). The raw data and processed data were deposited in Gene Expression Omnibus under accession
548 no. GSE157057. These datasets were analyzed here using various gene signatures.
549
550 **COVID-19 modeling in Syrian hamsters**
551 Lung samples from 8-week-old Syrian hamsters were generated from experiments conducted exactly as in a
552 previously published study(66). Animal studies were approved and performed in accordance with Scripps
553 Research IACUC Protocol #20-0003(66). We chose three different groups of samples: uninfected control, SARS-
554 CoV-2 challenge after Den3 (antibody to dengue virus), and SARS-CoV-2 challenge after Anti-CoV2 (CC12.2;
555 a potent SARS-CoV-2 neutralizing antibodies)(66).
556

557 **Immunohistochemistry**

558 COVID-19 samples were inactivated by storing in 10% formalin for 2 days and then transferred to zinc-formalin
559 solution for another 3 days. The deactivated tissues were transferred to 70% ethanol and cassettes were prepared
560 for tissue sectioning. The slides containing hamster and human lung tissue sections were deparaffinized in xylene
561 (Sigma-Aldrich Inc., MO, USA; catalog# 534056) and rehydrated in graded alcohols to water. For GRP78/ BIP,
562 p53, Cytokeratin 8, and Claudin 4-specific polyclonal antigen retrieval, slides were immersed in Tris-EDTA
563 buffer (pH 9.0) and boiled for 10 minutes at 100°C. Slides were immersed in Sodium Citrate Buffer (pH 6.0) and
564 boiled for 10 minutes at 100°C, for p14 ARF (E3X6D) and p21 Waf1/ Cip1(12D1) antigen retrieval. Endogenous
565 peroxidase activity was blocked by incubation with 3% H2O2 for 5-10 minutes. To block non-specific protein
566 binding either 2.5% goat or 2.5% horse serum (Vector Laboratories, Burlingame, USA; catalog# MP-7401 or S-
567 1012) was added. Tissues were then incubated with the following antibodies: rabbit GRP78/ BIP polyclonal
568 antibody (1:500 dilution; proteintech®, Rosemont, IL, USA; catalog# 11587-1-AP), rabbit p53 polyclonal
569 antibody (1:200 dilution ; proteintech®, Rosemont, IL, USA; catalog# 21891-1-AP), rabbit Cytokeratin 8
570 polyclonal antibody (1:2000 dilution; proteintech®, Rosemont, IL, USA; catalog# 10384-1-AP), and rabbit
571 Claudin 4-specific polyclonal antibody (1:200 dilution, proteintech®, Rosemont, IL, USA; catalog# 16195-1-AP)
572 for 1.5 hours at room temperature in a humidified chamber then rinsed with TBS twice for 3 minutes each.
573 Antibodies were prepared in antibody diluent (MP Biomedicals, LLC., Catalog # 980641) for rabbit p14 ARF
574 (E3X6D) monoclonal antibody (1:250 dilution; Cell Signaling Technology, Danvers, MA, USA; catalog#
575 74560S) and rabbit p21 Waf1/ Cip1 (12D1) monoclonal antibody (1:50 dilution; Cell Signaling Technology,
576 Danvers, MA, USA; catalog# 2947S) that were then incubated in a humidified chamber overnight at 4°C, then
577 rinsed with TBST twice for 5 minutes each. Sections were incubated with horse anti-rabbit (Vector Laboratories,
578 Burlingame, USA; catalog# MP-7401) secondary antibodies for 30 minutes at room temperature in a humidified
579 chamber and then washed with TBS or TBST 3x, 5 minutes each. Then incubated with DAB (BioGenex, Fremont,
580 CA, USA; catalog # HK542-XAKE) for 5-10 minutes and counterstained with hematoxylin (BioGenex, Fremont,
581 CA, USA; catalog# HK100-9K), dehydrated in graded alcohols, cleared in xylene, and cover slipped. All sides
582 were visualized by Leica DM1000 LED (Leica Microsystems, Germany).

583

584 **IHC Quantification**

585 IHC images were randomly sampled at different 300x300 pixel regions of interest (ROI). The ROIs were analyzed
586 using IHC Profiler(131). IHC Profiler uses a spectral deconvolution method of DAB/hematoxylin color spectra
587 by using optimized optical density vectors of the color deconvolution plugin for proper separation of the DAB
588 color spectra. The histogram of the DAB intensity was divided into 4 zones: high positive (0 to 60), positive (61
589 to 120), low positive (121 to 180) and negative (181 to 235). High positive, positive, and low positive percentages

were combined to compute the final percentage positive for each region of interest (ROI). The range of values for the percent positive is compared among different experimental groups.

Data availability

Source data are provided with this paper. All data is available in the main text or the supplementary materials. Publicly available datasets used are enlisted in **Supplemental Information 1**.

Code availability

The software codes are publicly available at the following links: https://github.com/sahoo00/BoNE(129) and https://github.com/sahoo00/Hegemon 86(130). The PPI network analysis can be found at: https://github.com/sinha7290/PPIN.

SUPPLEMENTARY MATERIALS:

- Detailed methods (text)
- Figures **3**
- Tables **0**
- Supplemental datasheets– **1-5**
- **Supplemental Information 1**: Excel datasheet with a list of transcriptomic datasets that were used in this work.
- **Supplemental Information 2**: Excel datasheet with gene expression signatures that were used in this work.
- **Supplemental Information 3**: COVID-19 patient demographics whose plasma were analyzed for cytokines.
- **Supplemental Information 4**: Cytokine expression profiles in COVID-19 patients vs healthy controls.
- **Supplemental Information 5**: Excel datasheet with list of degree sorted nodes in the protein-protein interaction network in **Fig 7B**.

620 **REFERENCES**

621 1. Spagnolo P, Balestro E, Aliberti S, Cocconcelli E, Biondini D, Casa GD, et al. Pulmonary fibrosis
622 secondary to COVID-19: a call to arms? Lancet Respir Med. 2020;8(8):750-2.
623 2. Myall KJ, Mukherjee B, Castanheira AM, Lam JL, Benedetti G, Mak SM, et al. Persistent Post-COVID-
624 19 Interstitial Lung Disease. An Observational Study of Corticosteroid Treatment. Ann Am Thorac Soc.
625 2021;18(5):799-806.
626 3. Wells AU, Devaraj A, Desai SR. Interstitial Lung Disease after COVID-19 Infection: A Catalog of
627 Uncertainties. Radiology. 2021;299(1):E216-e8.
628 4. Aronson KI, Podolanczuk AJ. Lungs after COVID-19: Evolving Knowledge of Post-COVID-19
629 Interstitial Lung Disease. Ann Am Thorac Soc. 2021;18(5):773-4.
630 5. Dadhwal R, Sharma M, Surani S. Restrictive Lung Disease in Patients With Subclinical Coronavirus
631 Infection: Are We Bracing Ourselves for Devastating Sequelae? Cureus. 2021;13(1):e12501.
632 6. Atabati E, Dehghani-Samani A, Mortazavimoghaddam SG. Association of COVID-19 and other viral
633 infections with interstitial lung diseases, pulmonary fibrosis, and pulmonary hypertension: A narrative review.
634 Can J Respir Ther. 2020;56:1-9.
635 7. Ahmad Alhiyari M, Ata F, Islam Alghizzawi M, Bint IBA, Salih Abdulhadi A, Yousaf Z. Post COVID-
636 19 fibrosis, an emerging complicationof SARS-CoV-2 infection. IDCases. 2021;23:e01041.
637 8. Alharthy A, Abuhamdah M, Balhamar A, Faqihi F, Nasim N, Ahmad S, et al. Residual Lung Injury in
638 Patients Recovering From COVID-19 Critical Illness: A Prospective Longitudinal Point-of-Care Lung
639 Ultrasound Study. J Ultrasound Med. 2020.
640 9. Gagiannis D, Steinestel J, Hackenbroch C, Schreiner B, Hannemann M, Bloch W, et al. Clinical,
641 Serological, and Histopathological Similarities Between Severe COVID-19 and Acute Exacerbation of
642 Connective Tissue Disease-Associated Interstitial Lung Disease (CTD-ILD). Front Immunol. 2020;11:587517.
643 10. George PM, Wells AU, Jenkins RG. Pulmonary fibrosis and COVID-19: the potential role for
644 antifibrotic therapy. Lancet Respir Med. 2020;8(8):807-15.
645 11. van Gassel RJJ, Bels J, Remij L, van Bussel BCT, Posthuma R, Gietema HA, et al. Functional
646 Outcomes and Their Association With Physical Performance in Mechanically Ventilated Coronavirus Disease
647 2019 Survivors at 3 Months Following Hospital Discharge: A Cohort Study. Crit Care Med. 2021.
648 12. Kaarteenaho R, Kinnula VL. Diffuse alveolar damage: a common phenomenon in progressive interstitial
649 lung disorders. Pulm Med. 2011;2011:531302.
650 13. Ackermann M, Verleden SE, Kuehnel M, Haverich A, Welte T, Laenger F, et al. Pulmonary Vascular
651 Endothelialitis, Thrombosis, and Angiogenesis in Covid-19. N Engl J Med. 2020;383(2):120-8.
652 14. Cheon IS, Li C, Son YM, Goplen NP, Wu Y, Cassmann T, et al. Immune signatures underlying post-
653 acute COVID-19 lung sequelae. Sci Immunol. 2021:eabk1741.
654 15. Bharat A, Querrey M, Markov NS, Kim S, Kurihara C, Garza-Castillon R, et al. Lung transplantation for
655 patients with severe COVID-19. Sci Transl Med. 2020;12(574).
656 16. Croci GA, Vaira V, Trabattoni D, Biasin M, Valenti L, Baselli G, et al. Emergency Lung
657 Transplantation after COVID-19: Immunopathological Insights on Two Affected Patients. Cells. 2021;10(3).
658 17. Bharat A, Machuca TN, Querrey M, Kurihara C, Garza-Castillon R, Jr., Kim S, et al. Early outcomes
659 after lung transplantation for severe COVID-19: a series of the first consecutive cases from four countries.
660 Lancet Respir Med. 2021;9(5):487-97.
661 18. Sahoo D, Katkar GD, Khandelwal S, Behroozikhah M, Claire A, Castillo V, et al. AI-guided discovery
662 of the invariant host response to viral pandemics. EBioMedicine. 2021;68:103390.
663 19. Levin M. Childhood Multisystem Inflammatory Syndrome - A New Challenge in the Pandemic. N Engl
664 J Med. 2020;383(4):393-5.
665 20. Sahoo D, Katkar GD, Shimizu C, Kim J, Khandelwal S, Tremoulet AH, et al. An AI-guided signature
666 reveals the nature of the shared proximal pathways of host immune response in MIS-C and Kawasaki disease.
667 Accepted, In Press, Nature Communication. 2021.

21. Imai Y, Kuba K, Rao S, Huan Y, Guo F, Guan B, et al. Angiotensin-converting enzyme 2 protects from severe acute lung failure. Nature. 2005;436(7047):112-6.
22. Bonham CA, Strek ME, Patterson KC. From granuloma to fibrosis: sarcoidosis associated pulmonary fibrosis. Curr Opin Pulm Med. 2016;22(5):484-91.
23. Patterson KC, Strek ME. Pulmonary fibrosis in sarcoidosis. Clinical features and outcomes. Ann Am Thorac Soc. 2013;10(4):362-70.
24. Meltzer EB, Barry WT, D'Amico TA, Davis RD, Lin SS, Onaitis MW, et al. Bayesian probit regression model for the diagnosis of pulmonary fibrosis: proof-of-principle. BMC Med Genomics. 2011;4:70.
25. Bauer Y, Tedrow J, de Bernard S, Birker-Robaczewska M, Gibson KF, Guardela BJ, et al. A novel genomic signature with translational significance for human idiopathic pulmonary fibrosis. Am J Respir Cell Mol Biol. 2015;52(2):217-31.
26. Gangwar I, Kumar Sharma N, Panzade G, Awasthi S, Agrawal A, Shankar R. Detecting the Molecular System Signatures of Idiopathic Pulmonary Fibrosis through Integrated Genomic Analysis. Sci Rep. 2017;7(1):1554.
27. Ammar R, Sivakumar P, Jarai G, Thompson JR. A robust data-driven genomic signature for idiopathic pulmonary fibrosis with applications for translational model selection. PLoS One. 2019;14(4):e0215565.
28. Lederer DJ, Martinez FJ. Idiopathic Pulmonary Fibrosis. N Engl J Med. 2018;378(19):1811-23.
29. Reyfman PA, Walter JM, Joshi N, Anekalla KR, McQuattie-Pimentel AC, Chiu S, et al. Single-Cell Transcriptomic Analysis of Human Lung Provides Insights into the Pathobiology of Pulmonary Fibrosis. Am J Respir Crit Care Med. 2019;199(12):1517-36.
30. Adams TS, Schupp JC, Poli S, Ayaub EA, Neumark N, Ahangari F, et al. Single-cell RNA-seq reveals ectopic and aberrant lung-resident cell populations in idiopathic pulmonary fibrosis. Sci Adv. 2020;6(28):eaba1983.
31. Xu G, Liu Y, Liao M, Gou J, Wang X, Yuan J, et al. Persistent viral activity, cytokine storm, and lung fibrosis in a case of severe COVID-19. Clin Transl Med. 2020;10(7):e224.
32. Wu X, Liu X, Zhou Y, Yu H, Li R, Zhan Q, et al. 3-month, 6-month, 9-month, and 12-month respiratory outcomes in patients following COVID-19-related hospitalisation: a prospective study. Lancet Respir Med. 2021;9(7):747-54.
33. Marshall M. The lasting misery of coronavirus long-haulers. Nature. 2020;585(7825):339-41.
34. Kølner-Augustson L, Prior TS, Skivild V, Aalestrup A, Bendstrup E. Fatigue in idiopathic pulmonary fibrosis measured by the Fatigue Assessment Scale during antifibrotic treatment. Eur Clin Respir J. 2020;8(1):1853658.
35. Bloem AEM, Mostard RLM, Stoot N, Vercoulen JH, Peters JB, Janssen DJA, et al. Severe Fatigue is Highly Prevalent in Patients with IPF or Sarcoidosis. J Clin Med. 2020;9(4).
36. Bloem AEM, Mostard RLM, Stoot N, Vercoulen JH, Peters JB, Spruit MA. Perceptions of fatigue in patients with idiopathic pulmonary fibrosis or sarcoidosis. J Thorac Dis. 2021;13(8):4872-84.
37. Herazo-Maya JD, Sun J, Molyneaux PL, Li Q, Villalba JA, Tzouvelekis A, et al. Validation of a 52-gene risk profile for outcome prediction in patients with idiopathic pulmonary fibrosis: an international, multicentre, cohort study. Lancet Respir Med. 2017;5(11):857-68.
38. van der Meer FJ, Orsel K, Barkema HW. The new influenza A H1N1 virus: balancing on the interface of humans and animals. Can Vet J. 2010;51(1):56-62.
39. Bermejo-Martin JF, Martin-Loeches I, Rello J, Antón A, Almansa R, Xu L, et al. Host adaptive immunity deficiency in severe pandemic influenza. Crit Care. 2010;14(5):R167.
40. Baden LR, Drazen JM, Kritek PA, Curfman GD, Morrissey S, Campion EW. H1N1 influenza A disease--information for health professionals. N Engl J Med. 2009;360(25):2666-7.
41. Zhong NS, Zheng BJ, Li YM, Poon, Xie ZH, Chan KH, et al. Epidemiology and cause of severe acute respiratory syndrome (SARS) in Guangdong, People's Republic of China, in February, 2003. Lancet. 2003;362(9393):1353-8.

716 42. Beigel JH, Farrar J, Han AM, Hayden FG, Hyer R, de Jong MD, et al. Avian influenza A (H5N1)
717 infection in humans. N Engl J Med. 2005;353(13):1374-85.
718 43. Zaki AM, van Boheemen S, Bestebroer TM, Osterhaus AD, Fouchier RA. Isolation of a novel
719 coronavirus from a man with pneumonia in Saudi Arabia. N Engl J Med. 2012;367(19):1814-20.
720 44. Zhai Y, Franco LM, Atmar RL, Quarles JM, Arden N, Bucasas KL, et al. Host Transcriptional Response
721 to Influenza and Other Acute Respiratory Viral Infections--A Prospective Cohort Study. PLoS Pathog.
722 2015;11(6):e1004869.
723 45. Liao M, Liu Y, Yuan J, Wen Y, Xu G, Zhao J, et al. Single-cell landscape of bronchoalveolar immune
724 cells in patients with COVID-19. Nat Med. 2020;26(6):842-4.
725 46. Wu K, Byers DE, Jin X, Agapov E, Alexander-Brett J, Patel AC, et al. TREM-2 promotes macrophage
726 survival and lung disease after respiratory viral infection. J Exp Med. 2015;212(5):681-97.
727 47. Evren E, Ringqvist E, Tripathi KP, Sleiers N, Rives IC, Alisjahbana A, et al. Distinct developmental
728 pathways from blood monocytes generate human lung macrophage diversity. Immunity. 2021;54(2):259-75.e7.
729 48. Leahy TR, McManus R, Doherty DG, Grealy R, Coulter T, Smyth P, et al. Interleukin-15 is associated
730 with disease severity in viral bronchiolitis. Eur Respir J. 2016;47(1):212-22.
731 49. Carson WE, Giri JG, Lindemann MJ, Linett ML, Ahdieh M, Paxton R, et al. Interleukin (IL) 15 is a
732 novel cytokine that activates human natural killer cells via components of the IL-2 receptor. J Exp Med.
733 1994;180(4):1395-403.
734 50. Zhang Z, Luo D, Zhong X, Choi JH, Ma Y, Wang S, et al. SCINA: A Semi-Supervised Subtyping
735 Algorithm of Single Cells and Bulk Samples. Genes (Basel). 2019;10(7).
736 51. Parimon T, Yao C, Stripp BR, Noble PW, Chen P. Alveolar Epithelial Type II Cells as Drivers of Lung
737 Fibrosis in Idiopathic Pulmonary Fibrosis. Int J Mol Sci. 2020;21(7).
738 52. Garcia CK. Insights from human genetic studies of lung and organ fibrosis. J Clin Invest.
739 2018;128(1):36-44.
740 53. Pardo A, Selman M. Molecular mechanisms of pulmonary fibrosis. Front Biosci. 2002;7:d1743-61.
741 54. Choi J, Park JE, Tsagkogeorga G, Yanagita M, Koo BK, Han N, et al. Inflammatory Signals Induce AT2
742 Cell-Derived Damage-Associated Transient Progenitors that Mediate Alveolar Regeneration. Cell Stem Cell.
743 2020;27(3):366-82.e7.
744 55. Strunz M, Simon LM, Ansari M, Kathiriya JJ, Angelidis I, Mayr CH, et al. Alveolar regeneration
745 through a Krt8+ transitional stem cell state that persists in human lung fibrosis. Nat Commun. 2020;11(1):3559.
746 56. Kobayashi Y, Tata A, Konkimalla A, Katsura H, Lee RF, Ou J, et al. Persistence of a regeneration-
747 associated, transitional alveolar epithelial cell state in pulmonary fibrosis. Nat Cell Biol. 2020;22(8):934-46.
748 57. Yao C, Guan X, Carraro G, Parimon T, Liu X, Huang G, et al. Senescence of Alveolar Type 2 Cells
749 Drives Progressive Pulmonary Fibrosis. Am J Respir Crit Care Med. 2021;203(6):707-17.
750 58. Abdelnabi R, Foo CS, Kaptein SJF, Zhang X, Do TND, Langendries L, et al. The combined treatment of
751 Molnupiravir and Favipiravir results in a potentiation of antiviral efficacy in a SARS-CoV-2 hamster infection
752 model. EBioMedicine. 2021;72:103595.
753 59. Cox RM, Wolf JD, Plemper RK. Therapeutically administered ribonucleoside analogue MK-
754 4482/EIDD-2801 blocks SARS-CoV-2 transmission in ferrets. Nat Microbiol. 2021;6(1):11-8.
755 60. Toots M, Yoon JJ, Cox RM, Hart M, Sticher ZM, Makhsous N, et al. Characterization of orally
756 efficacious influenza drug with high resistance barrier in ferrets and human airway epithelia. Sci Transl Med.
757 2019;11(515).
758 61. Toots M, Yoon JJ, Hart M, Natchus MG, Painter GR, Plemper RK. Quantitative efficacy paradigms of
759 the influenza clinical drug candidate EIDD-2801 in the ferret model. Transl Res. 2020;218:16-28.
760 62. Sheahan TP, Sims AC, Zhou S, Graham RL, Pruijssers AJ, Agostini ML, et al. An orally bioavailable
761 broad-spectrum antiviral inhibits SARS-CoV-2 in human airway epithelial cell cultures and multiple
762 coronaviruses in mice. Sci Transl Med. 2020;12(541).

63. Urakova N, Kuznetsova V, Crossman DK, Sokratian A, Guthrie DB, Kolykhalov AA, et al. β-d-N (4)-Hydroxycytidine Is a Potent Anti-alphavirus Compound That Induces a High Level of Mutations in the Viral Genome. J Virol. 2018;92(3).
64. Abdelnabi R, Foo CS, Kaptein SJF, Zhang X, Langendries L, Vangeel L, et al. Molnupiravir (EIDD-2801) inhibits SARS-CoV-2 replication and enhances the efficacy of favipiravir in a Syrian hamster infection model. bioRxiv. 2021:2020.12.10.419242.
65. Fischer W, Eron JJ, Holman W, Cohen MS, Fang L, Szewczyk LJ, et al. Molnupiravir, an Oral Antiviral Treatment for COVID-19. medRxiv. 2021.
66. Rogers TF, Zhao F, Huang D, Beutler N, Burns A, He WT, et al. Isolation of potent SARS-CoV-2 neutralizing antibodies and protection from disease in a small animal model. Science. 2020;369(6506):956-63.
67. Yang P, Gu H, Zhao Z, Wang W, Cao B, Lai C, et al. Angiotensin-converting enzyme 2 (ACE2) mediates influenza H7N9 virus-induced acute lung injury. Sci Rep. 2014;4:7027.
68. Vasarmidi E, Tsitoura E, Spandidos DA, Tzanakis N, Antoniou KM. Pulmonary fibrosis in the aftermath of the COVID-19 era (Review). Exp Ther Med. 2020;20(3):2557-60.
69. Pang J, Xu F, Aondio G, Li Y, Fumagalli A, Lu M, et al. Efficacy and tolerability of bevacizumab in patients with severe Covid-19. Nat Commun. 2021;12(1):814.
70. Tindle C, Fuller M, Fonseca A, Taheri S, Ibeawuchi SR, Beutler N, et al. Adult stem cell-derived complete lung organoid models emulate lung disease in COVID-19. Elife. 2021;10.
71. Lamers MM, van der Vaart J, Knoops K, Riesebosch S, Breugem TI, Mykytyn AZ, et al. An organoid-derived bronchioalveolar model for SARS-CoV-2 infection of human alveolar type II-like cells. EMBO J. 2021;40(5):e105912.
72. Szklarczyk D, Gable AL, Nastou KC, Lyon D, Kirsch R, Pyysalo S, et al. The STRING database in 2021: customizable protein-protein networks, and functional characterization of user-uploaded gene/measurement sets. Nucleic Acids Res. 2021;49(D1):D605-D12.
73. In-Yee Lee and Jan-Ming Ho and Ming-Syan C. CLUGO: a clustering algorithm for automated functional annotations based on gene ontology. 2005. p. 4 -.
74. Fabregat A, Jupe S, Matthews L, Sidiropoulos K, Gillespie M, Garapati P, et al. The Reactome Pathway Knowledgebase. Nucleic Acids Res. 2018;46(D1):D649-D55.
75. Barrett TJ, Cornwell M, Myndzar K, Rolling CC, Xia Y, Drenkova K, et al. Platelets amplify endotheliopathy in COVID-19. Sci Adv. 2021;7(37):eabh2434.
76. Bonaventura A, Vecchié A, Dagna L, Martinod K, Dixon DL, Van Tassell BW, et al. Endothelial dysfunction and immunothrombosis as key pathogenic mechanisms in COVID-19. Nat Rev Immunol. 2021;21(5):319-29.
77. Maruhashi T, Higashi Y. Pathophysiological Association of Endothelial Dysfunction with Fatal Outcome in COVID-19. Int J Mol Sci. 2021;22(10).
78. Senchenkova EY, Komoto S, Russell J, Almeida-Paula LD, Yan LS, Zhang S, et al. Interleukin-6 mediates the platelet abnormalities and thrombogenesis associated with experimental colitis. Am J Pathol. 2013;183(1):173-81.
79. Nosaka M, Ishida Y, Kimura A, Kuninaka Y, Taruya A, Ozaki M, et al. Crucial Involvement of IL-6 in Thrombus Resolution in Mice via Macrophage Recruitment and the Induction of Proteolytic Enzymes. Front Immunol. 2019;10:3150.
80. Borok Z, Horie M, Flodby P, Wang H, Liu Y, Ganesh S, et al. Loss in Epithelial Progenitors Reveals an Age-linked Role for Endoplasmic Reticulum Stress in Pulmonary Fibrosis. Am J Respir Crit Care Med. 2020;201(2):198-211.
81. Rock JR, Barkauskas CE, Cronce MJ, Xue Y, Harris JR, Liang J, et al. Multiple stromal populations contribute to pulmonary fibrosis without evidence for epithelial to mesenchymal transition. Proc Natl Acad Sci U S A. 2011;108(52):E1475-83.
82. Barkauskas CE, Cronce MJ, Rackley CR, Bowie EJ, Keene DR, Stripp BR, et al. Type 2 alveolar cells are stem cells in adult lung. J Clin Invest. 2013;123(7):3025-36.

83. Frank DB, Peng T, Zepp JA, Snitow M, Vincent TL, Penkala IJ, et al. Emergence of a Wave of Wnt Signaling that Regulates Lung Alveologenesis by Controlling Epithelial Self-Renewal and Differentiation. Cell Rep. 2016;17(9):2312-25.
84. Zhou J, Mao B, Zhou Q, Ding D, Wang M, Guo P, et al. Endoplasmic reticulum stress activates telomerase. Aging Cell. 2014;13(1):197-200.
85. Sanchez-Vazquez R, Guío-Carrión A, Zapatero-Gaviria A, Martínez P, Blasco MA. Shorter telomere lengths in patients with severe COVID-19 disease. Aging (Albany NY). 2021;13(1):1-15.
86. Aviv A. Short telomeres and severe COVID-19: The connection conundrum. EBioMedicine. 2021;70:103513.
87. Verheyden JM, Sun X. A transitional stem cell state in the lung. Nat Cell Biol. 2020;22(9):1025-6.
88. Liu RM, Liu G. Cell senescence and fibrotic lung diseases. Exp Gerontol. 2020;132:110836.
89. Parimon T, Hohmann MS, Yao C. Cellular Senescence: Pathogenic Mechanisms in Lung Fibrosis. Int J Mol Sci. 2021;22(12).
90. Sahoo D, Katkar GD, Shimizu C, Kim J, Khandelwal S, Tremoulet AH, et al. An AI-guided signature reveals the nature of the shared proximal pathways of host immune response in MIS-C and Kawasaki disease. bioRxiv. 2021.
91. Gaddam RR, Chambers S, Bhatia M. ACE and ACE2 in inflammation: a tale of two enzymes. Inflamm Allergy Drug Targets. 2014;13(4):224-34.
92. Inlay MA, Bhattacharya D, Sahoo D, Serwold T, Seita J, Karsunky H, et al. Ly6d marks the earliest stage of B-cell specification and identifies the branchpoint between B-cell and T-cell development. Genes Dev. 2009;23(20):2376-81.
93. Sodhi CP, Nguyen J, Yamaguchi Y, Werts AD, Lu P, Ladd MR, et al. A Dynamic Variation of Pulmonary ACE2 Is Required to Modulate Neutrophilic Inflammation in Response to. J Immunol. 2019;203(11):3000-12.
94. Jia H. Pulmonary Angiotensin-Converting Enzyme 2 (ACE2) and Inflammatory Lung Disease. Shock. 2016;46(3):239-48.
95. Kuba K, Imai Y, Penninger JM. Multiple functions of angiotensin-converting enzyme 2 and its relevance in cardiovascular diseases. Circ J. 2013;77(2):301-8.
96. Esposito AJ, Menon AA, Ghosh AJ, Putman RK, Fredenburgh LE, El-Chemaly SY, et al. Increased Odds of Death for Patients with Interstitial Lung Disease and COVID-19: A Case-Control Study. Am J Respir Crit Care Med. 2020;202(12):1710-3.
97. Drake TM, Docherty AB, Harrison EM, Quint JK, Adamali H, Agnew S, et al. Outcome of Hospitalization for COVID-19 in Patients with Interstitial Lung Disease. An International Multicenter Study. Am J Respir Crit Care Med. 2020;202(12):1656-65.
98. Podolanczuk AJ, Richeldi L. COVID-19 and Interstitial Lung Disease: Keep Them Separate. Am J Respir Crit Care Med. 2020;202(12):1614-6.
99. Gallay L, Uzunhan Y, Borie R, Lazor R, Rigaud P, Marchand-Adam S, et al. Risk Factors for Mortality after COVID-19 in Patients with Preexisting Interstitial Lung Disease. Am J Respir Crit Care Med. 2021;203(2):245-9.
100. FIRDAUS H, RAZAK NA, REZA M, KHAN NA, SHAMEEM M. Clinical Improvement with Pirfenidone in Two Patients of COVID 19. Journal of Clinical & Diagnostic Research. 2020;14(12).
101. Momen ABI, Khan F, Saber S, Sultana A, Alam RF, Raihan SG, et al. Usefulness of Pirfenidone in Covid Lung: A Case Series. European Journal of Medical and Health Sciences. 2021;3(1):24-6.
102. Xi Z, Zhigang Z, Ting L. Post-inflammatory pulmonary fibrosis in a discharged COVID-19 patient: Effectively treated with Pirfenidone. Archives of Pulmonology and Respiratory Care. 2020;6(1):051-3.
103. McGonagle D, Sharif K, O'Regan A, Bridgewood C. The Role of Cytokines including Interleukin-6 in COVID-19 induced Pneumonia and Macrophage Activation Syndrome-Like Disease. Autoimmun Rev. 2020;19(6):102537.
104. . !!! INVALID CITATION !!! (93).

105. Muro S, Taha R, Tsicopoulos A, Olivenstein R, Tonnel AB, Christodoulopoulos P, et al. Expression of IL-15 in inflammatory pulmonary diseases. J Allergy Clin Immunol. 2001;108(6):970-5.
106. Takada T, Ohashi K, Hayashi M, Asakawa K, Sakagami T, Kikuchi T, et al. Role of IL-15 in interstitial lung diseases in amyopathic dermatomyositis with anti-MDA-5 antibody. Respir Med. 2018;141:7-13.
107. Wuttge DM, Wildt M, Geborek P, Wollheim FA, Scheja A, Akesson A. Serum IL-15 in patients with early systemic sclerosis: a potential novel marker of lung disease. Arthritis Res Ther. 2007;9(5):R85.
108. Alder JK, Barkauskas CE, Limjunyawong N, Stanley SE, Kembou F, Tuder RM, et al. Telomere dysfunction causes alveolar stem cell failure. Proc Natl Acad Sci U S A. 2015;112(16):5099-104.
109. Abdul-Careem MF, Mian MF, Yue G, Gillgrass A, Chenoweth MJ, Barra NG, et al. Critical role of natural killer cells in lung immunopathology during influenza infection in mice. J Infect Dis. 2012;206(2):167-77.
110. Schneider WM, Chevillotte MD, Rice CM. Interferon-stimulated genes: a complex web of host defenses. Annu Rev Immunol. 2014;32:513-45.
111. Froidure A, Mahieu M, Hoton D, Laterre PF, Yombi JC, Koenig S, et al. Short telomeres increase the risk of severe COVID-19. Aging (Albany NY). 2020;12(20):19911-22.
112. McGroder CF, Zhang D, Choudhury MA, Salvatore MM, D'Souza BM, Hoffman EA, et al. Pulmonary fibrosis 4 months after COVID-19 is associated with severity of illness and blood leucocyte telomere length. Thorax. 2021.
113. Mongelli A, Barbi V, Gottardi Zamperla M, Atlante S, Forleo L, Nesta M, et al. Evidence for Biological Age Acceleration and Telomere Shortening in COVID-19 Survivors. Int J Mol Sci. 2021;22(11).
114. Katzen J, Beers MF. Contributions of alveolar epithelial cell quality control to pulmonary fibrosis. J Clin Invest. 2020;130(10):5088-99.
115. Borok Z, Horie M, Flodby P, Wang H, Liu Y, Ganesh S, et al. Grp78 Loss in Epithelial Progenitors Reveals an Age-linked Role for Endoplasmic Reticulum Stress in Pulmonary Fibrosis. Am J Respir Crit Care Med. 2020;201(2):198-211.
116. Liang J, Zhang Y, Xie T, Liu N, Chen H, Geng Y, et al. Hyaluronan and TLR4 promote surfactant-protein-C-positive alveolar progenitor cell renewal and prevent severe pulmonary fibrosis in mice. Nat Med. 2016;22(11):1285-93.
117. Xu Y, Mizuno T, Sridharan A, Du Y, Guo M, Tang J, et al. Single-cell RNA sequencing identifies diverse roles of epithelial cells in idiopathic pulmonary fibrosis. JCI Insight. 2016;1(20):e90558.
118. Chilosi M, Carloni A, Rossi A, Poletti V. Premature lung aging and cellular senescence in the pathogenesis of idiopathic pulmonary fibrosis and COPD/emphysema. Transl Res. 2013;162(3):156-73.
119. Chen H, Chen H, Liang J, Gu X, Zhou J, Xie C, et al. TGF-β1/IL-11/MEK/ERK signaling mediates senescence-associated pulmonary fibrosis in a stress-induced premature senescence model of Bmi-1 deficiency. Exp Mol Med. 2020;52(1):130-51.
120. Rana T, Jiang C, Liu G, Miyata T, Antony V, Thannickal VJ, et al. PAI-1 Regulation of TGF-β1-induced Alveolar Type II Cell Senescence, SASP Secretion, and SASP-mediated Activation of Alveolar Macrophages. Am J Respir Cell Mol Biol. 2020;62(3):319-30.
121. Evangelou K, Veroutis D, Foukas PG, Paschalaki K, Lagopati N, Dimitriou M, et al. SARS-CoV-2 infects lung epithelial cells and induces senescence and an inflammatory response in patients with severe COVID-19. bioRxiv. 2021:2021.01.02.424917.
122. Lee S, Yu Y, Trimpert J, Benthani F, Mairhofer M, Richter-Pechanska P, et al. Virus-induced senescence is a driver and therapeutic target in COVID-19. Nature. 2021;599(7884):283-9.
123. Lipskaia L, Maisonnasse P, Fouillade C, Sencio V, Pascal Q, Flaman JM, et al. Evidence that SARS-CoV-2 Induces Lung-Cell Senescence: Potential Impact on COVID-19 Lung Disease. Am J Respir Cell Mol Biol. 2021.
124. D'Agnillo F, Walters KA, Xiao Y, Sheng ZM, Scherler K, Park J, et al. Lung epithelial and endothelial damage, loss of tissue repair, inhibition of fibrinolysis, and cellular senescence in fatal COVID-19. Sci Transl Med. 2021;13(620):eabj7790.

910 125. Fink G, Orlova-Fink N, Schindler T, Grisi S, Ferrer APS, Daubenberger C, et al. Inactivated trivalent
911 influenza vaccination is associated with lower mortality among patients with COVID-19 in Brazil. BMJ Evid
912 Based Med. 2020.
913 126. Wagstaffe HR, Pickering H, Houghton J, Mooney JP, Wolf AS, Prevatt N, et al. Influenza Vaccination
914 Primes Human Myeloid Cell Cytokine Secretion and NK Cell Function. J Immunol. 2019;203(6):1609-18.
915 127. Hoek KL, Samir P, Howard LM, Niu X, Prasad N, Galassie A, et al. A cell-based systems biology
916 assessment of human blood to monitor immune responses after influenza vaccination. PLoS One.
917 2015;10(2):e0118528.
918 128. Carson WE, Ross ME, Baiocchi RA, Marien MJ, Boiani N, Grabstein K, et al. Endogenous production
919 of interleukin 15 by activated human monocytes is critical for optimal production of interferon-gamma by
920 natural killer cells in vitro. J Clin Invest. 1995;96(6):2578-82.
921 129. Sahoo D, Dill DL, Gentles AJ, Tibshirani R, Plevritis SK. Boolean implication networks derived from
922 large scale, whole genome microarray datasets. Genome Biol. 2008;9(10):R157.
923 130. Sahoo D, Seita J, Bhattacharya D, Inlay MA, Weissman IL, Plevritis SK, et al. MiDReG: a method of
924 mining developmentally regulated genes using Boolean implications. Proc Natl Acad Sci U S A.
925 2010;107(13):5732-7.
926 131. Varghese F, Bukhari AB, Malhotra R, De A. IHC Profiler: an open source plugin for the quantitative
927 evaluation and automated scoring of immunohistochemistry images of human tissue samples. PLoS One.
928 2014;9(5):e96801.
929 132. Dabydeen SA, Desai A, Sahoo D. Unbiased Boolean analysis of public gene expression data for cell
930 cycle gene identification. Mol Biol Cell. 2019;30(14):1770-9.
931 133. Sahoo D, Dill DL, Tibshirani R, Plevritis SK. Extracting binary signals from microarray time-course
932 data. Nucleic Acids Res. 2007;35(11):3705-12.
933 134. Ju Z, Jiang H, Jaworski M, Rathinam C, Gompf A, Klein C, et al. Telomere dysfunction induces
934 environmental alterations limiting hematopoietic stem cell function and engraftment. Nat Med. 2007;13(6):742-
935 7.

936
937

938 ## AUTHOR CONTRIBUTIONS

939 DS, SS and PG conceptualized the project; SS and DS carried out all computational modeling and analyses and
940 DS contributed all software used in this work; GDK carried out the human serum cytokine analysis; VC and SS
941 carried out the immunohistochemical studies and their quantitative analysis under the supervision of PG; AGF
942 carried out the immunofluorescence studies on COVID-19 lung tissues; SS carried out the PPI network creation
943 and analysis; JD provided access to human subjects for cytokine analyses. CT, CRE and SD were responsible for
944 the COVID-19 lung models. SS, DS and PG prepared figures for data visualization; SS and PG wrote the original
945 draft of the manuscript; DS, SD, GK edited and revised the manuscript. All co-authors approved the final version
946 of the manuscript. DS, SD, and PG supervised various parts of the project and secured funding; DS and PG
947 administered the project.

948

949 ## DECLARATION OF INTERESTS

950 The authors declare no competing interests.

951

952 ## ACKNOWLEDGEMENTS

953 This work was supported by the National Institutes for Health (NIH) grants R00-CA151673 and R01-GM138385
954 (to DS) and R01-AI141630, CA100768 and CA160911 (to P.G), R01DK107585 (SD) and R01-AI155696 (to
955 P.G, D.S and S.D), UCOP-RGPO (R00RG2628 & R00RG2642 to P.G, D.S and S.D). GDK was supported
956 through the American Association of Immunologists Intersect Fellowship Program for Computational Scientists
957 and Immunologists. JMD was supported by U19AI142742. We thank Zea Borok (UCSD) for helpful discussions
958 during the preparation of this manuscript.

959

960 **Data sharing:**

961 All data is available in the main text or the supplementary materials.

962

963 **FIGURES AND LEGENDS**

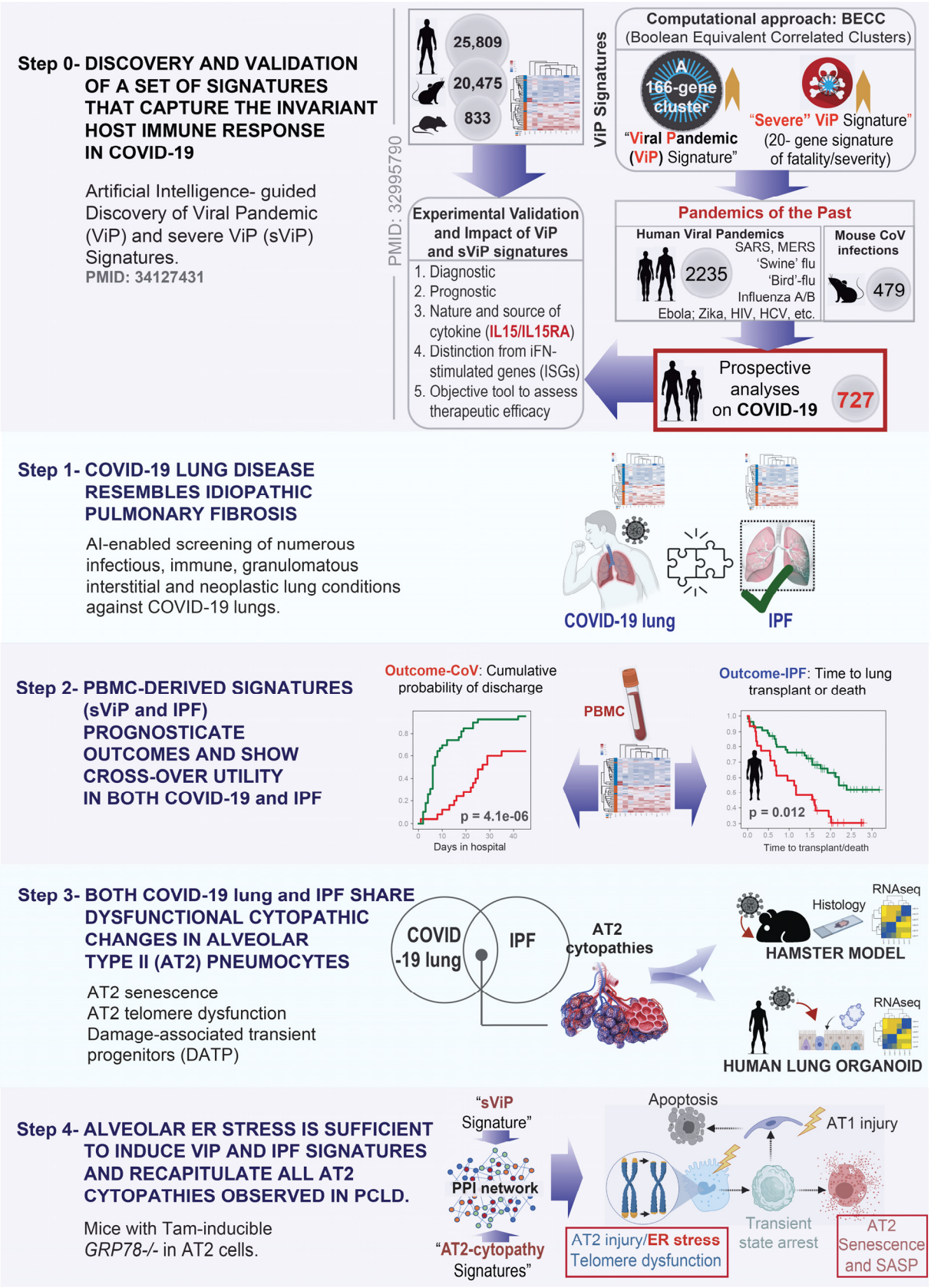

964

965 **Figure 1. Study design: Artificial Intelligence-guided navigation of COVID-19 lung disease.**

(*From top to bottom*) *Step 0*: Over 45,000 human, mouse, and rat gene expression databases were mined using machine learning tools called Boolean Equivalent Correlated Clusters (BECC(132)) to identify invariant host response to viral pandemics (ViP). In the absence of a sufficiently large number of COVID-19 datasets at the onset of the COVID-19 pandemic, these ViP signatures were trained on only two datasets from the pandemics of the past (Influenza and avian flu; GSE47963, n = 438; GSE113211, n = 118) and used without further training to prospectively analyze the samples from the current pandemic (i.e., COVID-19; n = 727 samples from diverse datasets). A subset of 20-genes classified disease severity called severe-ViP (sViP) signature. The ViP signatures appeared to capture the 'invariant' host response, i.e., the shared fundamental nature of the host immune response induced by all viral pandemics, including COVID-19. *Step1*: The set of ViP/sViP signatures and a CoV-lung specific(13) gene signature was analyzed on diverse transcriptomic datasets representing a plethora of lung diseases; these efforts identified COVID-19 lung disease to be the closest to Idiopathic pulmonary fibrosis (IPF); both conditions induced a common array of gene signatures. *Step 2*: Clinically useful whole-blood and PBMC-derived prognostic signatures previously validated in IPF(37) showed crossover efficacy in COVID-19, and *vice versa*. *Step 3*: Gene signatures of alveolar type II (AT2) cytopathic changes that are known to fuel IPF were analyzed in COVID-19 lung, and predicted shared features were validated in human and hamster lungs and lung-organoid derived models. *Step 4:* Protein- protein interaction (PPI) network built using sViP and AT2 cytopathy-related signatures was analyzed to pinpoint ER stress as a major shared feature in COVID-19 lung disease and IPF, which was subsequently validated in human and hamster lungs.

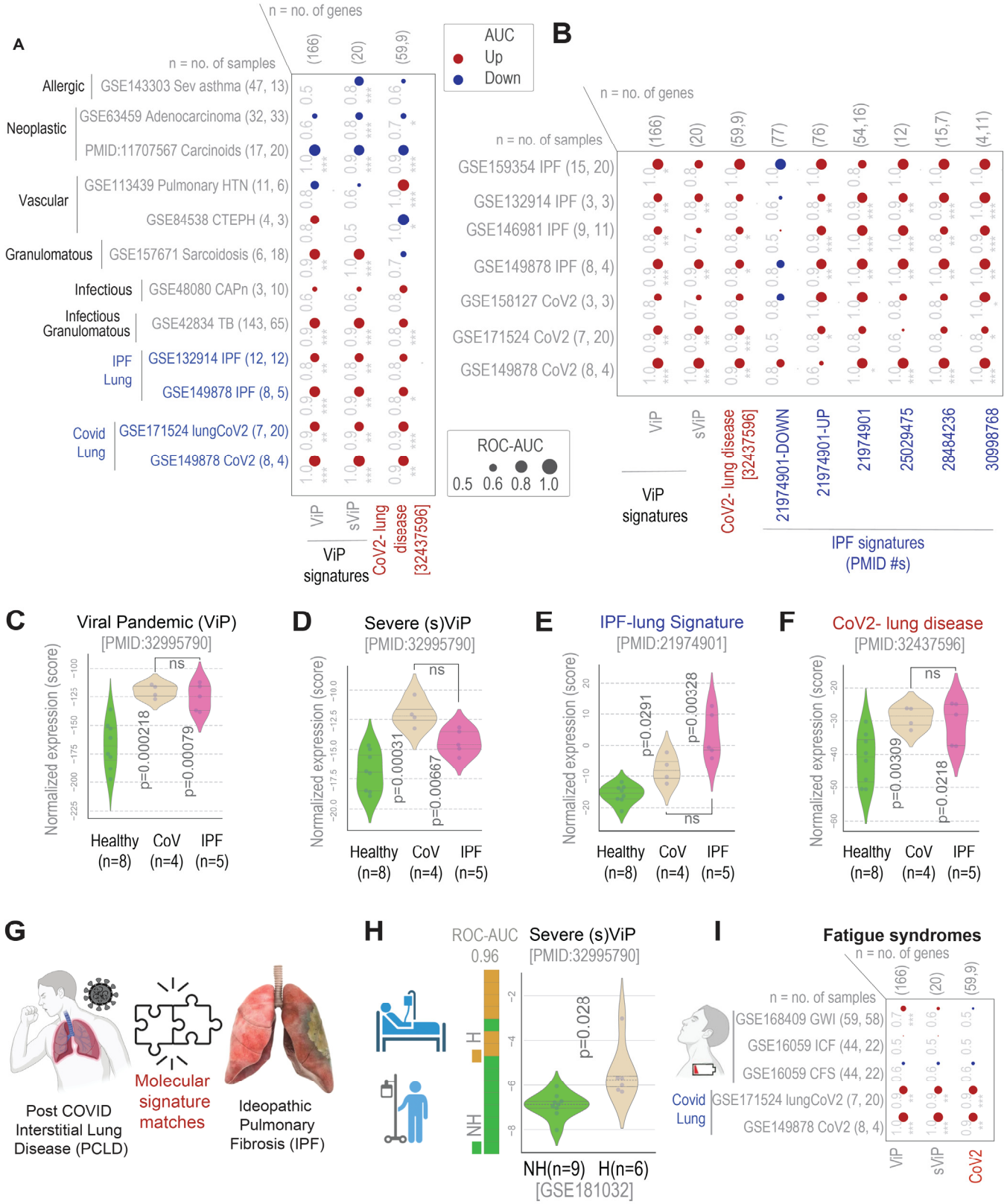

Figure 2. Identification of lung condition(s) that resemble COVID-19 lung disease.

A. Bubble plots show the ROC-AUC values (radii of circles are based on the ROC-AUC) show the direction of gene regulation (Up, red; Down, blue) for sample classification based on the induction of ViP/sViP(18) and a previously published human CoV-lung signatures(13) in diverse datasets representing diverse lung pathologies, including COVID-19. Tuberculosis, TB; community acquired pneumonia, CAPn; pulmonary hypertension, PHT; chronic thromboembolic pulmonary hypertension, CTEPH; idiopathic pulmonary fibrosis, IPF; CoV, COVID-19. **B.** Bubble plots in B show the ROC-AUC values for sample classification based on the induction of ViP signatures and several previously published IPF signatures in COVID-19 infected lungs and sc-RNA seq datasets from IPF explants. **C-F.** Violin plots display the extent of induction of ViP (E) or sViP (F), IPF (G) or CoV lung (H) signatures in a pooled cohort of healthy, CoV and IPF lung samples (GSE149878; GSE122960). Welch's two sample unpaired t-test is performed on the composite gene signature score (z-score of normalized tpm count) to compute the *p* values. In multi-group setting each group is compared to the first control group and only significant *p* values are displayed. **G.** Schematic summarizes the predicted molecular match between COVID-19 lung and IPF based on the crossover validation of gene signatures showcased in B-F. **H.** Bar plots show the ability of sViP signature to classify COVID-19 patients based on hospitalization status and violin plots show the degree of induction of the signature within each group (H, hospitalized; NH, non-hospitalized). Welch's two sample unpaired t-test is performed on the composite gene signature score (z-score of normalized tpm count) to compute the *p values*. **I.** Bubble plots of ROC-AUC values (radii of circles are based on the ROC-AUC) show the direction of gene regulation (Up, red; Down, blue) for the classification of healthy vs diseased samples based on the ViP/sViP and the CoV-lung signatures on three well known fatigue conditions (blood/PBMC samples from GWI, gulf war illness; CFS, chronic fatigue syndrome).

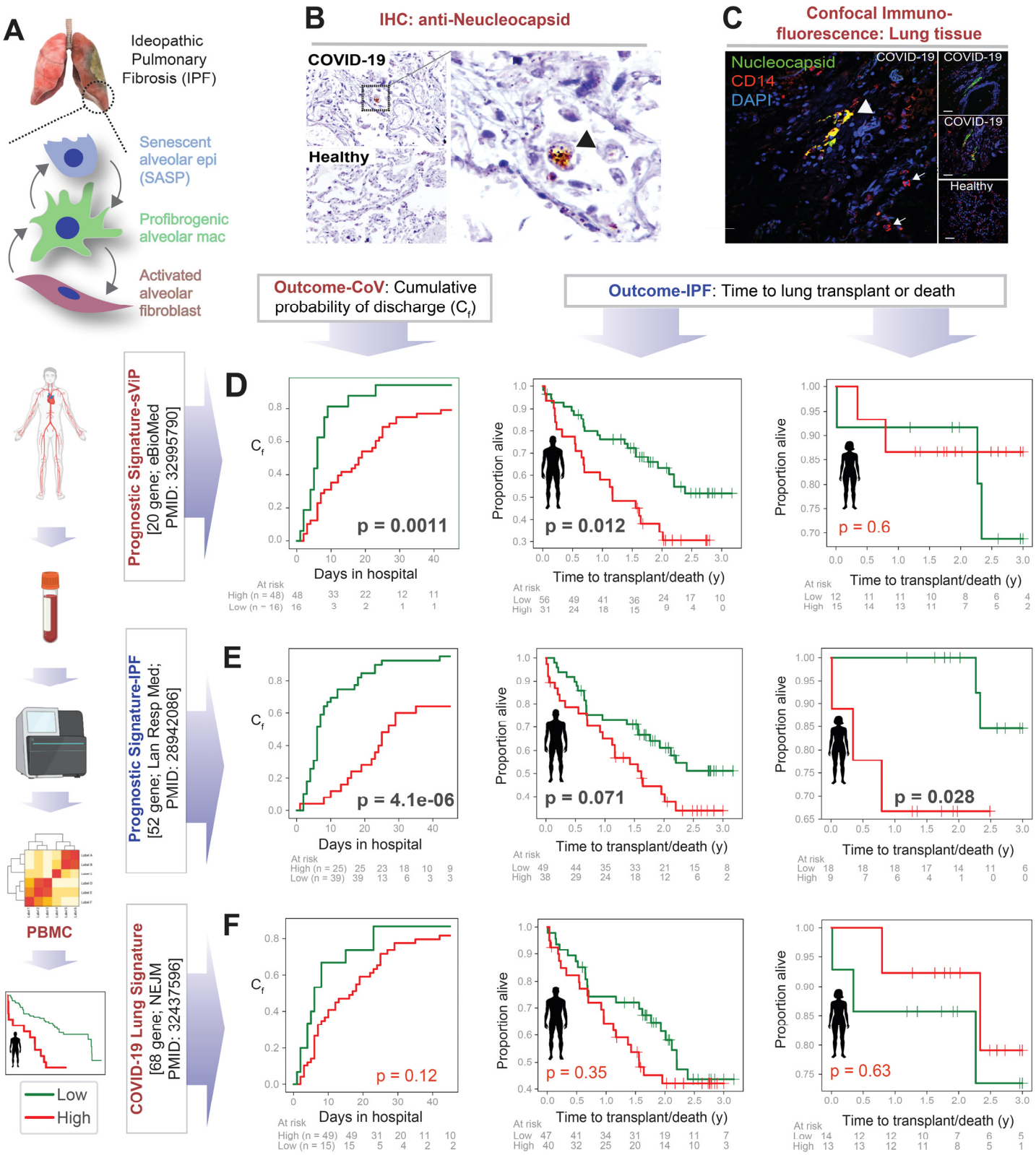

Figure 3. PBMC-derived prognostic signatures in IPF also prognosticate outcome in COVID-19.

1012 **A.** Schematic showing the current understanding of the complex interplay between senescent alveolar
1013 pneumocyte (AT2), reactive alveolar macrophage, and fibroblasts in the pathogenesis of pulmonary fibrosis. **B-**
1014 **C**. FFPE tissues from normal lungs and from the lungs of subjects deceased due to COVID-19 were analyzed
1015 for the SARS-CoV2 viral nucleocapsid protein either by IHC (B) or by confocal immunofluorescence (C). Lungs
1016 were co-stained also with CD14 (a marker for activated alveolar macrophage(47)) in C. **D.** Kaplan-Meier plots
1017 show the stratification of patients based on the degree of induction of the sViP signature in PBMCs (low and high
1018 group; determined using the StepMiner algorithm(133) and its relationship to either the cumulative probability of
1019 discharge of COVID-19 patients (D-*left*; GSE157103; derived from the hospital-free days during a 45-day follow-
1020 up), or the time to lung transplant or death in male (D-*middle*) and female (D-*right*) IPF patients (GSE28221).
1021 Statistical significances were estimated using the log rank test. **E.** Kaplan-Meier plots on the same cohorts as in
1022 D, using a PBMC-derived 52-gene IPF-specific prognostic signature that was previously validated on numerous
1023 independent IPF cohorts(37). **F**. Kaplan-Meier plots on the same cohorts as in D-E, using a CoV-lung derived
1024 signature.

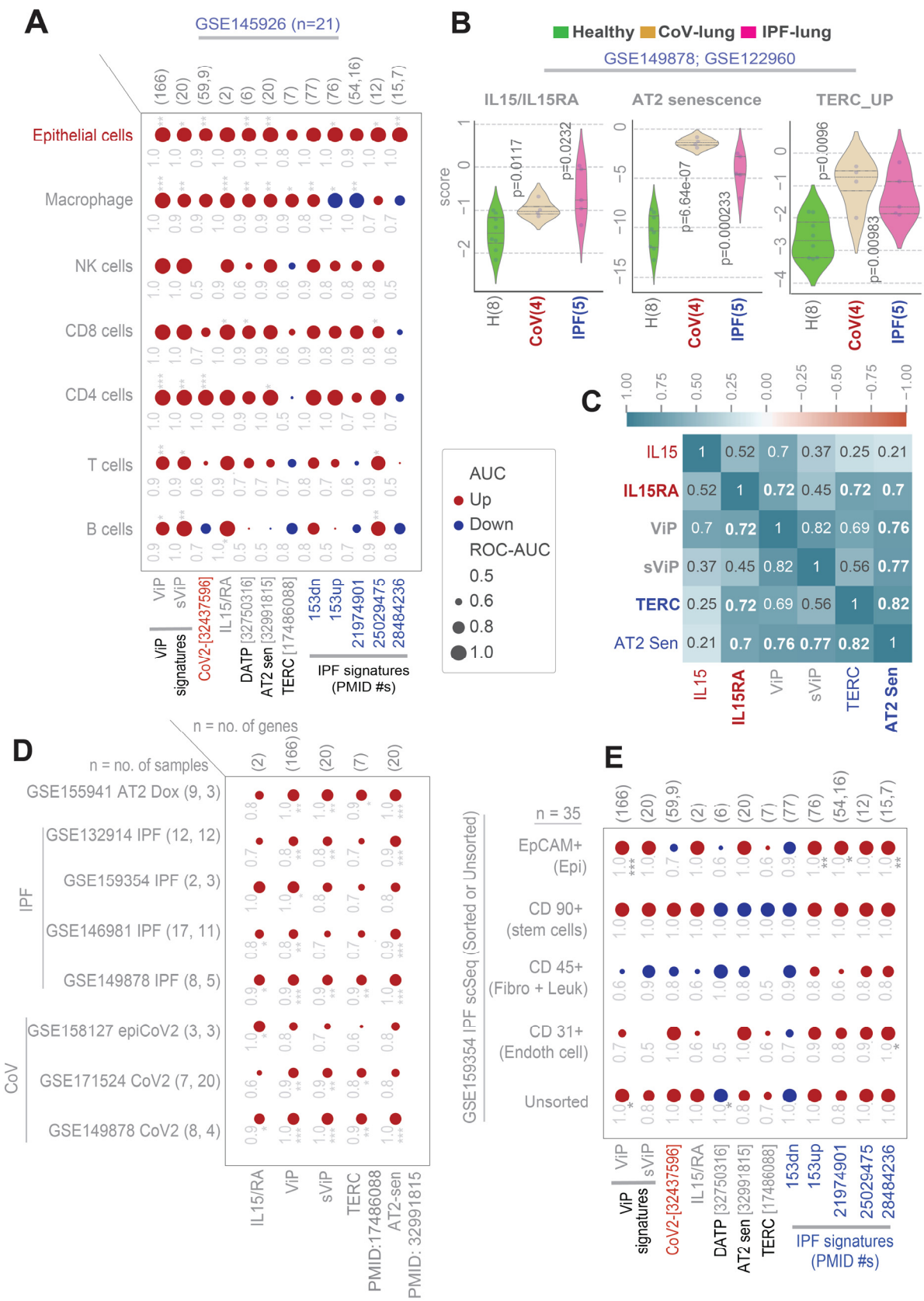

Figure 4. Identification of shared AT2 cytopathies in COVID-19 and IPF.

A. Bubble plot of ROC-AUC values (radii of circles are based on the ROC-AUC) demonstrating the direction of gene regulation (Up, red; Down, blue) for the classification of various cell types between healthy and CoV lung based on various ViP/sViP and IPF gene signatures in **Fig 2A-B** alongside *IL15/IL15RA* and additional signatures of AT2 cytopathies that are encountered and implicated in IPF (DATP, damage associated transient progenitors; Sens, senescence; TERC, *Te*lomerase *R*NA *C*omponent). Numbers in parenthesis indicate PMIDs. **B.** Violin plots display the extent of induction of a *IL15/IL15RA* composite score (B-*left*), or a signature of AT2 senescence(57) (B-*middle*), or a gene set for telomere dysfunction (JU_AGING_TERC(134)) in a pooled cohort of healthy, CoV and IPF lung samples (GSE149878; GSE122960). Welch's two sample unpaired t-test is performed on the composite gene signature score (z-score of normalized tpm count) to compute the *p* values. In multi-group setting each group is compared to the first control group and only significant p values are displayed. **C.** Correlation matrix showing the Pearson's correlation coefficient between different gene signatures in the pooled healthy, CoV and IPF lung dataset (GSE149878; GSE122960). **D.** Bubble plots of ROC-AUC values (radii of circles are based on the ROC-AUC) demonstrating the direction of gene regulation (Up, red; Down, blue) for the classification based on AT2 senescence-related signatures on other publicly available CoV and IPF bulk RNA seq datasets. **E.** Bubble plots of ROC-AUC values (radii of circles are based on the ROC-AUC) demonstrating the direction of gene regulation (Up, red; Down, blue) for different types of cells in an independent sc-RNA seq datasets of IPF explants and healthy lung tissues.

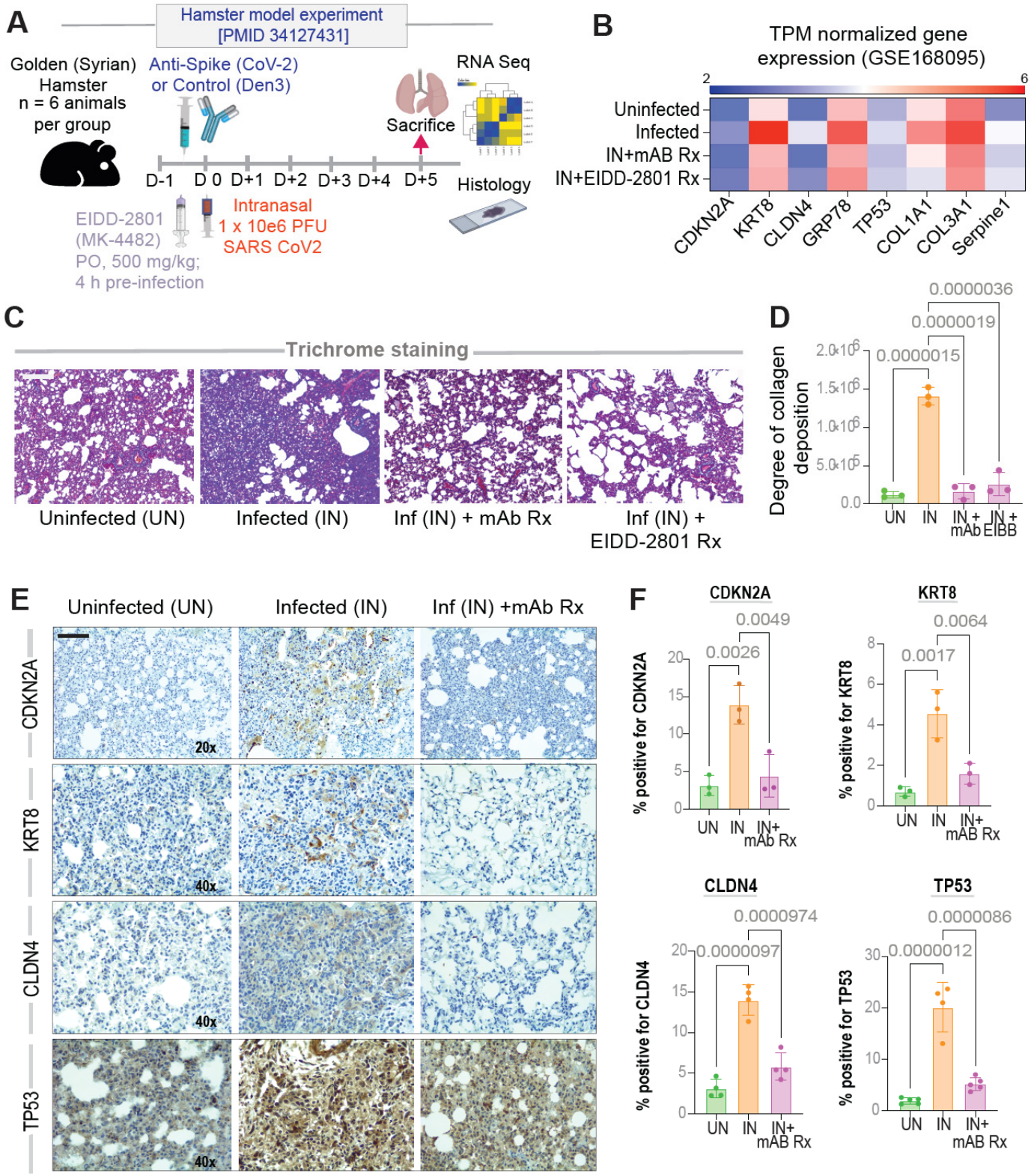

Figure 5. SARS-CoV-2-challenged hamster lungs faithfully recapitulate AT2 cytopathies in COVID-19.

1048 **A.** Schematic showing the experimental design for COVID-19 modeling in golden Syrian hamsters. *Uninf*,
1049 uninfected; *Den3 and Anti-CoV-2* indicate SARS-CoV-2 challenged groups that received either a control mAb or
1050 the clone CC12.2 of anti-CoV-2 IgG(66), respectively. PFU, plaque-forming units. **B**. Heatmap showing
1051 transcripts/million (TPM)-normalized gene expression of specific genes associated with AT2 senescence
1052 (*CDKN2A*, *TP53*), damage associated transition state progenitor (DATP) arrested state (*CLDN4*, *KRT8*), ER stress
1053 (*HSPA5*/*GRP78*) and SASP-state (*SERPINE1*, *COL1A*, *COL3A*). **C-D**. Lungs harvested from the uninfected,
1054 infected, and infected but anti-CoV-2 IgG and infected but EIDD-2801 treated hamsters have been analyzed for
1055 the abundance of collagen deposition by Trichrome staining and quantified by ImageJ. Representative images are
1056 shown panel C. Scale bar = 200 µm. Results of the quantification are displayed as bar plot in D. Statistical
1057 significance was analyzed by one way ANOVA. Error bars represent S.E.M; n = 3. **E-F**. Lungs harvested from
1058 the uninfected, infected, and infected but anti-CoV-2 IgG groups were analyzed by IHC for the indicated proteins
1059 and quantified by ImageJ- IHC profiler. Representative images are shown panel E. Scale bar = 200 µm. Results
1060 of the quantification are displayed as violin plots in F. Statistical significance was analyzed by one way ANOVA;
1061 n = 4.

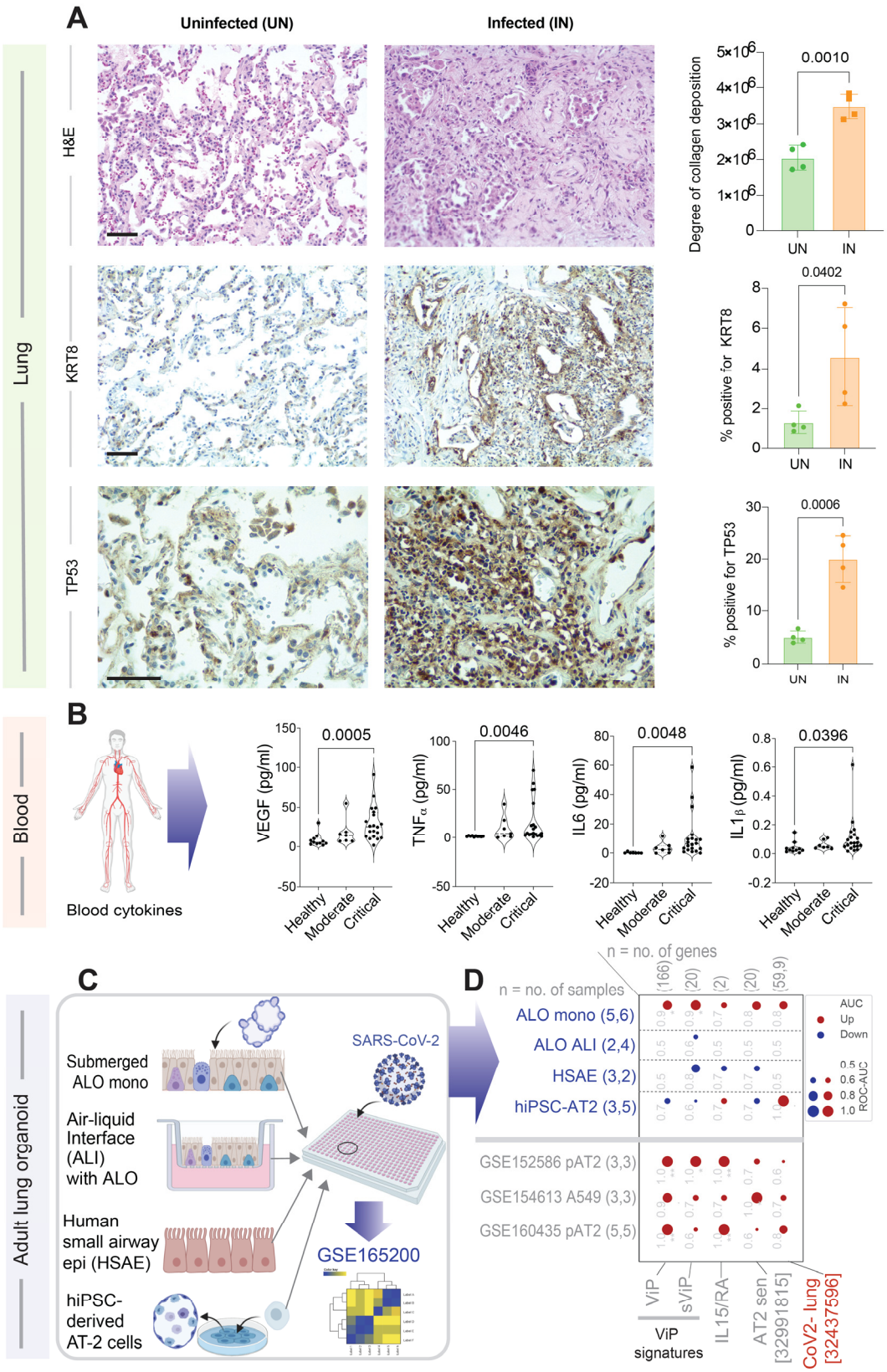

Figure 6. AT2 cytopathic features of IPF are detected in COVID-19 lung tissues and human pre-clinical organoid models of COVID-19.

1065 **A**. FFPE lung tissues collected during rapid autopsy of deceased COVID-19-infected subjects and histologically
1066 normal surgically resected lung tissues were analyzed by H&E staining (*top*) and for the expression of KRT8 (a
1067 marker of DATP(54); *middle*) and TP53 (a marker of senescence; *bottom*) by IHC. Representative fields are
1068 shown on the left. Scale bar = 200 µm. Images were quantified by IHC profiler (ImageJ) and displayed as violin
1069 plots on the right. **B**. Violin plots display the abundance of key senescence-associated cytokines in the plasma
1070 from adults with COVID-19 and healthy volunteers. Statistical significance was analyzed by unpaired t-test. See
1071 also **Supplemental Information 3-4** for patient demographics and cytokine concentrations. **C-D**. Schematic in
1072 C summarizes the various pre-clinical *in vitro* models of the human lung that were challenged with SARS-CoV-
1073 2, followed by RNA sequencing(70) (*top* rows; blue font; D). Other independent SARS-CoV-2-challenged
1074 alveolar pneumocyte datasets are listed in grey font (D). Bubble plots in D show the ROC-AUC values (radii of
1075 circles are based on the ROC-AUC) demonstrating the direction of gene regulation (Up, red; Down, blue) for the
1076 classification of uninfected vs infected samples based on the signatures (below).

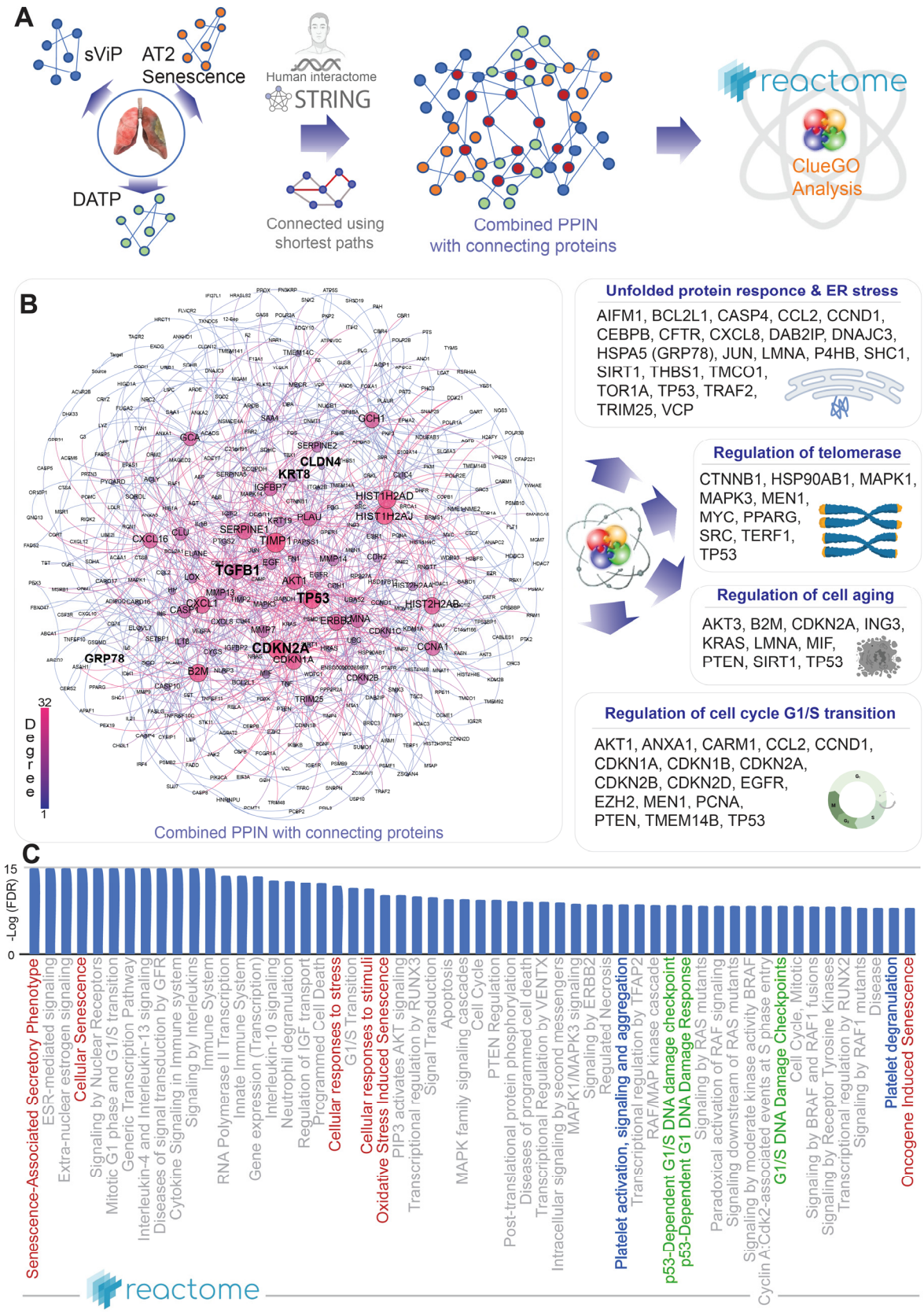

Figure 7. Protein-protein interaction network (PPIN) analysis predicts ER stress in AT2 cells as a driver pathophysiology in COVID-19

1080 **A**. Schematic summarizes the key steps in building a PPI network using as 'seeds' the genes in the sVIP, AT2
1081 senescence and transition state arrest (DATP) signatures and connecting them using shortest paths prior to
1082 carrying out network analyses. **B**. The combined PPI network is shown on the left and the degree of connectivity
1083 is indicated. See also **Supplemental Information 5** for the complete list of nodes sorted by their degrees of
1084 connectivity. Schematics on the right summarize the results of CluGo analysis, which identifies cellular processes
1085 and key genes that may perpetuate lung fibrosis. **C**. Reactome pathway analysis of the PPI network lists the most
1086 significant pathways that are associated with the node list in the network in B. Red = senescence related processes;
1087 Green = DNA damage response pathways; Blue = Platelet activation and degranulation.

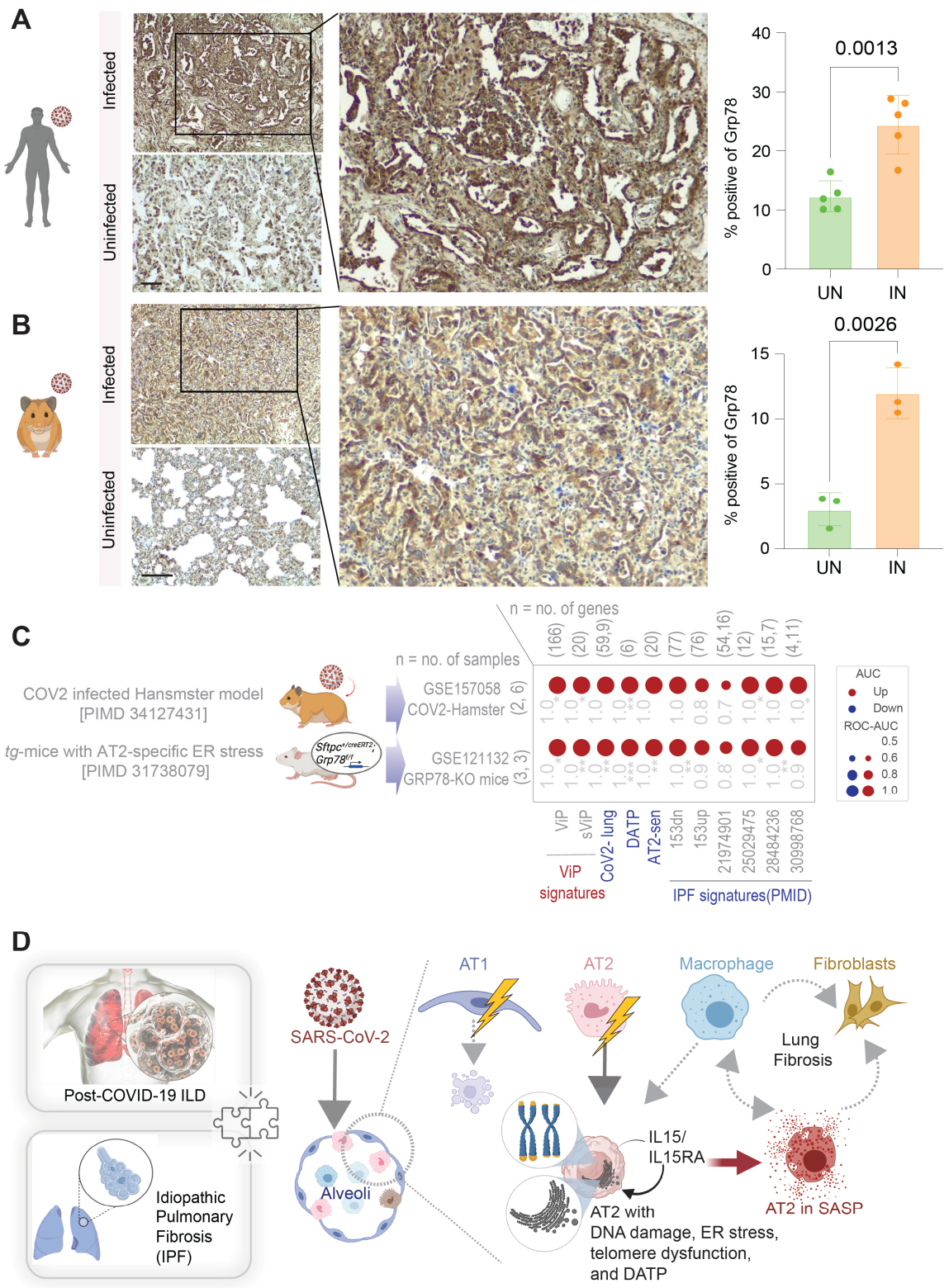

Figure 8. Induction of ER stress in AT2 cells is observed in COVID-19 and is sufficient to mimic the host immune response in COVID-19 and IPF

1091 **A-B**. FFPE uninfected (control) and SARS-CoV-2-infected human (A) and hamster (B) lungs were analyzed for
1092 GRP78 expression by IHC. Representative fields are shown on the left. Scale bar = 200 μm. Images were
1093 quantified by IHC profiler (ImageJ) and displayed as violin plots on the right. **C**. Bubble plots show the ROC-
1094 AUC values (radii of circles are based on the ROC-AUC) demonstrating the direction of gene regulation (Up,
1095 red; Down, blue) for the classification of WT vs *GRP78*-KO murine lung (bottom row) and uninfected vs. infected
1096 hamster lung (top row) samples based on the signatures (below). **D**. Schematic summarizes the findings in this
1097 work and the proposed working model for the contributions of various alveolar cells in fueling the fibrotic
1098 progression in both IPF and COVID-19.